Human Molecular Genetics, 2016, Vol. 25, No. 10 2045–2059

doi: 10.1093/hmg/ddw078
Advance Access Publication Date: 2 March 2016
Original Article

ORIGINAL ARTICLE

Heterozygous mutation of *Ush1g/Sans* in mice causes early-onset progressive hearing loss, which is recovered by reconstituting the strain-specific mutation in *Cdh23*†

Yuki Miyasaka[1,3], Hiroshi Shitara[2,5], Sari Suzuki[1], Sachi Yoshimoto[2,5], Yuta Seki[1], Yasuhiro Ohshiba[1,3], Kazuhiro Okumura[6], Choji Taya[2], Hisashi Tokano[7], Ken Kitamura[7], Toyoyuki Takada[8], Hiroshi Hibino[4], Toshihiko Shiroishi[8], Ryo Kominami[3], Hiromichi Yonekawa[2] and Yoshiaki Kikkawa[1,3,*]

[1]Mammalian Genetics Project, [2]Laboratory for Transgenic Technology, Tokyo Metropolitan Institute of Medical Science, Tokyo 156-8506, Japan, [3]Graduate School of Medical and Dental Sciences, [4]Department of Molecular Physiology, Niigata University School of Medicine, Niigata 951-8510, Japan, [5]Graduate School of Life and Environmental Sciences, University of Tsukuba, Tsukuba 305-8572, Japan, [6]Division of Oncogenomics, Cancer Genome Center, Chiba Cancer Center Research Institute, Chiba 260-0801, Japan, [7]Department of Otolaryngology, Tokyo Medical and Dental University, Tokyo 113-0034, Japan and [8]Mammalian Genetics Laboratory, National Institute of Genetics, Mishima 411-8540, Japan

*To whom correspondence should be addressed at: Mammalian Genetics Project, Tokyo Metropolitan Institute of Medical Science, 2-1-6 Kami-kitazawa, Setagaya-ku, Tokyo 156-8506, Japan. Tel: +81 3 5316 3311; Fax: +81 3 5316 3311; Email: kikkawa-ys@igakuken.or.jp

Abstract

Most clinical reports have suggested that patients with congenital profound hearing loss have recessive mutations in deafness genes, whereas dominant alleles are associated with progressive hearing loss (PHL). Jackson shaker (*Ush1g*^{js}) is a mouse model of recessive deafness that exhibits congenital profound deafness caused by the homozygous mutation of *Ush1g/Sans* on chromosome 11. We found that C57BL/6J-*Ush1g*$^{js/+}$ heterozygous mice exhibited early-onset PHL (ePHL) accompanied by progressive degeneration of stereocilia in the cochlear outer hair cells. Interestingly, ePHL did not develop in mutant mice with the C3H/HeN background, thus suggesting that other genetic factors are required for ePHL development. Therefore, we performed classical genetic analyses and found that the occurrence of ePHL in *Ush1g*$^{js/+}$ mice was associated with an interval in chromosome 10 that contains the cadherin 23 gene (*Cdh23*), which is also responsible for human deafness. To confirm this mutation effect, we generated C57BL/6J-*Ush1g*$^{js/+}$, *Cdh23*$^{c.753A/G}$ double-heterozygous mice by using the CRISPR/Cas9-mediated *Cdh23*$^{c.753A>G}$ knock-in method. The *Cdh23*$^{c.753A/G}$ mice harbored a one-base substitution (A for G), and the homozygous A allele caused moderate hearing loss with aging. Analyses revealed the complete recovery of ePHL and stereocilia degeneration in C57BL/6J-*Ush1g*$^{js/+}$ mice. These results clearly show that the development of ePHL requires at least two mutant alleles of the *Ush1g* and *Cdh23* genes. Our results also suggest that because the SANS and CDH23 proteins form a complex in the stereocilia, the interaction between these proteins may play key roles in the maintenance of stereocilia and the prevention of ePHL.

†GenBank Accession Nos LC094966–094979.

Received: December 13, 2015. **Revised:** February 19, 2016. **Accepted:** February 29, 2016

Introduction

Usher syndrome (USH) is a condition characterized by syndromic hearing loss accompanied by retinitis pigmentosa and vestibular dysfunction, and it is the most common cause of deaf-blindness in humans (1,2). USH is classified into three clinical subtypes, USH1–3, on the basis of the onset of hearing loss, retinitis pigmentosa and the absence of vestibular function (1,2). Mutations in 11 genes have been identified in patients with these subtypes (1–3), and all of these genes encode proteins that localize to the stereocilia of the inner ear hair cells (4–11). Interestingly, 9 of these 11 mutant genes have been identified in mouse models, and mice with homozygous mutations in these genes exhibit balance defects and profound congenital hearing loss caused by the disorganization of stereocilia (4,5,7,9,10,12–17).

It is generally assumed that the symptoms of USH patients are recessively inherited because mono- and biallelic mutations in the *USH* causative genes have been identified in patients (1–3). Moreover, homozygous loss-of-function mutations in seven *USH* genes, myosin VIIa (*MYO7A*) (18), Usher syndrome 1C (*USH1C*/*Harmonin*) (19), cadherin 23 (*CDH23*) (20), protocadherin 15 (*PCDH15*) (21), Usher syndrome 1G (*USH1G*/*SANS*) (22), calcium and integrin-binding family member 2 (*CIB2*) (11), and deafness, autosomal recessive 31 (*DFNB31*/*Whirlin*) (23), also cause autosomal recessive nonsyndromic hearing loss (NSHL). Notably, heterozygotes may also develop hearing loss. DFNA11, a well-known autosomal dominant NSHL disorder, is caused by a mutation in one *MYO7A* allele (24–26). Moreover, some patients with progressive NSHL have heterozygous mutations in *USH1C* (27), *CDH23* (27,28) and *PCDH15* (29). More importantly, different heterozygotes show differing times of NSHL onset, which probably depends on the effects of various other genes and mutations.

Several reports have indicated that the time of onset of hearing loss and the degree of its severity vary in heterozygous patients carrying a similar mutation in the same deafness causative gene (e.g. 30–33). Classical genetic theories, including haploinsufficiency, dominant-negative effects and gain-of-function effects, cannot simply explain this variability. In addition, the penetrance in dominant NSHL is generally lower than that in the recessive disorder (34–36). These findings suggest that one or more genetic factors, other than single-allele mutations, are required for the development of hearing loss. The effects of other genes and combinations of allelic mutations can be predicted in humans by using next-generation sequencing (NGS) technologies (37). However, the combination of allelic mutations cannot be experimentally confirmed in humans because many candidate pathogenic mutations are usually detected in NSHL patients by mutation screening using NGS (37). Furthermore, if the phenotypes are different, the status of mutations cannot be resolved in NSHL patients even if the mutations are detected in known deafness genes. Therefore, mouse models are indispensable for resolving these issues. Because the similar structures of the human and mouse auditory systems are conserved (36,38), it is possible to elucidate the effects of mutations by phenotypic analysis of mouse models with alterations that precisely mimic mutations identified in NSHL patients. In particular, the recently developed knock-in (KI) system via the transcription activator-like effector nuclease (TALEN) and clustered regularly interspaced short palindromic repeat (CRISPR)-associated Cas9 nuclease (CRISPR/Cas9) genome editing can efficiently and quickly produce these mimicking mutations (39).

In this paper, we present an *in vivo* analysis of the dominant effect of the *Ush1g* single mutant allele on chromosome 11 of hearing loss and of an additive effect when this mutation is combined with the homozygous *Cdh23* mutation (40) on chromosome 10 in the genetic background of a mouse model for hearing loss, Jackson shaker (*Ush1g*^{js}) (13,14). We found that *Ush1g*^{js} heterozygous mice exhibited early-onset progressive hearing loss (ePHL) and age-dependent cochlear outer hair cell (OHC) degeneration. The additive effect was detected and confirmed using quantitative trait locus (QTL) mapping and the CRISPR/Cas9-mediated KI method, respectively. The results indicated that genetic and molecular mechanisms contribute to hearing loss and the accompanying cochlear degeneration in mice carrying heterozygous mutant alleles in two deafness genes, and these findings are probably applicable to humans as well.

Results

Hearing assessments of *Ush1g*$^{js/+}$ heterozygous mice

The *Ush1g*^{js} mutation is a frame-shift mutation (p.Glu228ArgfsX9) that results in a truncated SANS protein lacking the C-terminal SAM domain (13). *Ush1g*$^{js/js}$ homozygous mice exhibit typical shaker/waltzer behavior, such as circling, head tossing and hyperactivity (13,14). The behavior of B6J-*Ush1g*$^{js/+}$ heterozygous mice was normal, as demonstrated by open-field behavior tests (Supplementary Material, Fig. S1), and this and other behavioral phenotypes did not change with age. The hearing ability of B6J-*Ush1g*$^{js/+}$ heterozygous mice, however, was affected and appeared abnormal following examination of the auditory brain stem responses (ABRs) evoked by tone-pip stimuli at 4, 8, 16 and 32 kHz. The presence of measurable thresholds at 2 months of age in B6J-*Ush1g*$^{+/+}$ and -*Ush1g*$^{js/+}$ mice allowed us to determine the latency peak response for Peaks I–V at various frequencies, whereas the B6J-*Ush1g*$^{js/js}$ mice failed to show ABRs (Supplementary Material, Fig. S2). At 6 months of age, the amplitudes of the peaks at all frequencies were clearly reduced in B6J-*Ush1g*$^{js/+}$ mice compared with B6J-*Ush1g*$^{+/+}$ mice (Fig. 1A). In particular, we could barely detect the ABR waveform peaks using maximum sound pressures at 16 and 32 kHz. We next determined the ABR thresholds for tone-pip stimuli at 4, 8, 16 and 32 kHz in B6J-*Ush1g*$^{js/+}$ mice at 1–12 months of age at 1-month intervals and compared them with our previous data from the B6J-*Ush1g*$^{+/+}$ mice (15). This analysis revealed a clear increase in ABR thresholds in the B6J-*Ush1g*$^{js/+}$ mice. In response to stimuli at 4 and 8 kHz, the ABR thresholds among the B6J-*Ush1g*$^{js/+}$ mice gradually changed from 4 to 5 months of age, and their hearing impairment increased in severity over time (Fig. 1B and Supplementary Material, Table S1). Significant differences in ABR thresholds at 16 and 32 kHz were first observed between *Ush1g*$^{+/+}$ and *Ush1g*$^{js/+}$ mice at 1 month of age, and the ABR thresholds in *Ush1g*$^{js/+}$ mice rapidly reached a level that was indicative of severe (71–90 decibel sound pleasure level: dB SPL) (34) and profound (<90 dB SPL) hearing impairment when compared with *Ush1g*$^{+/+}$ mice (Fig. 1B and Supplementary Material, Table S1). These results suggest that *Ush1g*$^{js/+}$ heterozygous mice exhibit an ePHL that is more severe for high-frequency stimuli (Fig. 1 and Supplementary Material, Fig. S2).

C3H/HeN (C3H) mice carry another spontaneous *Ush* mutation, *Ush1g*^{seal}, which is also a frame-shift mutation (p.Thr398SerfsX52) that results in a truncated protein without the C-terminal SAM domain of the SANS protein (13). We determined the ABR thresholds in C3H-*Ush1g*$^{seal/+}$ and C3H-*Ush1g*$^{+/+}$ mice at 1–12 months of age. There were no significant differences between the two types of mice, except for responses to 4 and 32 kHz in aged mice (8 and 9 months of age), and the C3H-*Ush1g*$^{seal/+}$ mice did not exhibit onset of ePHL, at least up to 12 months of age (Fig. 1B and Supplementary Material, Table S1). Although differences in the phenotypes

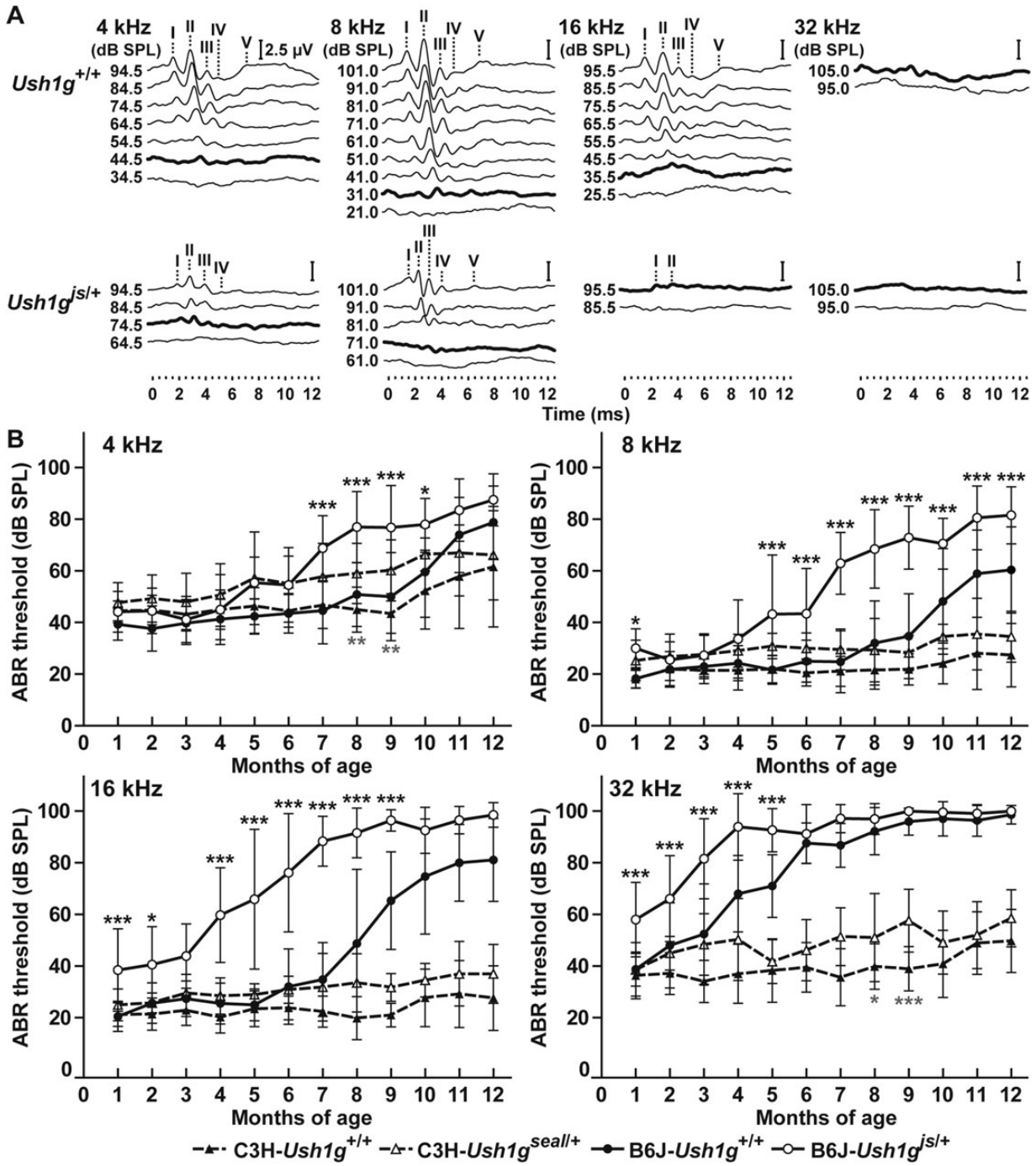

Figure 1. Early-onset PHL in B6J-*Ush1g*$^{js/+}$ heterozygous mice. (**A**) Representative ABR waveforms from B6J-*Ush1g*$^{+/+}$ and -*Ush1g*$^{js/+}$ heterozygous mice at 6 months of age. The waveforms represent the ABR in response to tone-pip stimuli at 4, 8, 16 and 32 kHz. The bold lines represent the thresholds detected. The locations of Peaks I–V are indicated. Scale bars = 2.5 μV. (**B**) The means (circles and upper triangles) and SDs (error bars) of ABR threshold measurements for 4, 8, 16 and 32 kHz stimuli are shown for B6J-*Ush1g*$^{+/+}$, -*Ush1g*$^{js/+}$, C3H-*Ush1g*$^{+/+}$ and -*Ush1g*$^{seal/+}$ mice at 1–12 months of age. The data for ABR threshold measurements in B6J-*Ush1g*$^{+/+}$ mice are cited from our previous study (15). The data for ABR thresholds are listed in Supplementary Material, Table S1. The upper black and lower gray asterisks indicate significant differences (*$P < 0.05$, **$P < 0.01$ and ***$P < 0.001$) between the ABR thresholds for B6J-*Ush1g*$^{+/+}$ versus -*Ush1g*$^{js/+}$ and in C3H-*Ush1g*$^{+/+}$ versus -*Ush1g*$^{seal/+}$ mice, respectively.

between the B6J-*Ush1g*$^{js/+}$ and C3H-*Ush1g*$^{seal/+}$ mice are likely due to the different mutations, our results showed that the ePHL phenotype will occur with the presence of a single *Ush1g*^{js} allele in the B6J genetic background, suggesting that ePHL is accelerated by the additive effect between *Ush1g*^{js} and B6J-derived genetic modifiers.

Identification of a susceptibility modifier for the onset of ePHL in B6J-*Ush1g*$^{js/+}$ heterozygous mice

To analyze the effects of the B6J genetic background on ePHL in *Ush1g*$^{js/+}$ heterozygous mice, we produced F_1 mice and backcrossed progeny with MSM/Ms (MSM) mice, which maintain stable hearing throughout their lives (41); we then measured

the ABR thresholds to 16 and 32 kHz stimuli at 4 months of age. The average ABR thresholds (22.0 ± 6.7 dB SPL at 16 kHz and 32.0 ± 7.5 dB SPL at 32 kHz) of (MSM × B6J-*Ush1g*$^{js/js}$) F_1 mice were not significantly different from those of MSM mice (Fig. 2A). The average ABR thresholds at 16 and 32 kHz of *Ush1g*$^{js/+}$ heterozygotes from the (MSM × B6J-*Ush1g*$^{js/js}$) F_1 × B6J-*Ush1g*$^{js/js}$ intersubspecific backcross progeny (N_2) mice were 40.4 ± 22.2 and 59.1 ± 27.9 dB SPL, respectively. The distribution of ABR thresholds at 16 kHz stimuli in the *Ush1g*$^{js/+}$ heterozygous backcross mice followed the predicted distribution (Fig. 2B), appearing as a bimodal scatter with the first group displaying thresholds of <35.0 dB SPL (55.0%). The second group exhibited thresholds greater than 35.0 dB SPL (45.0%), as classified on the basis of the mean thresholds from the *Ush1g*$^{js/+}$ heterozygous MSM and

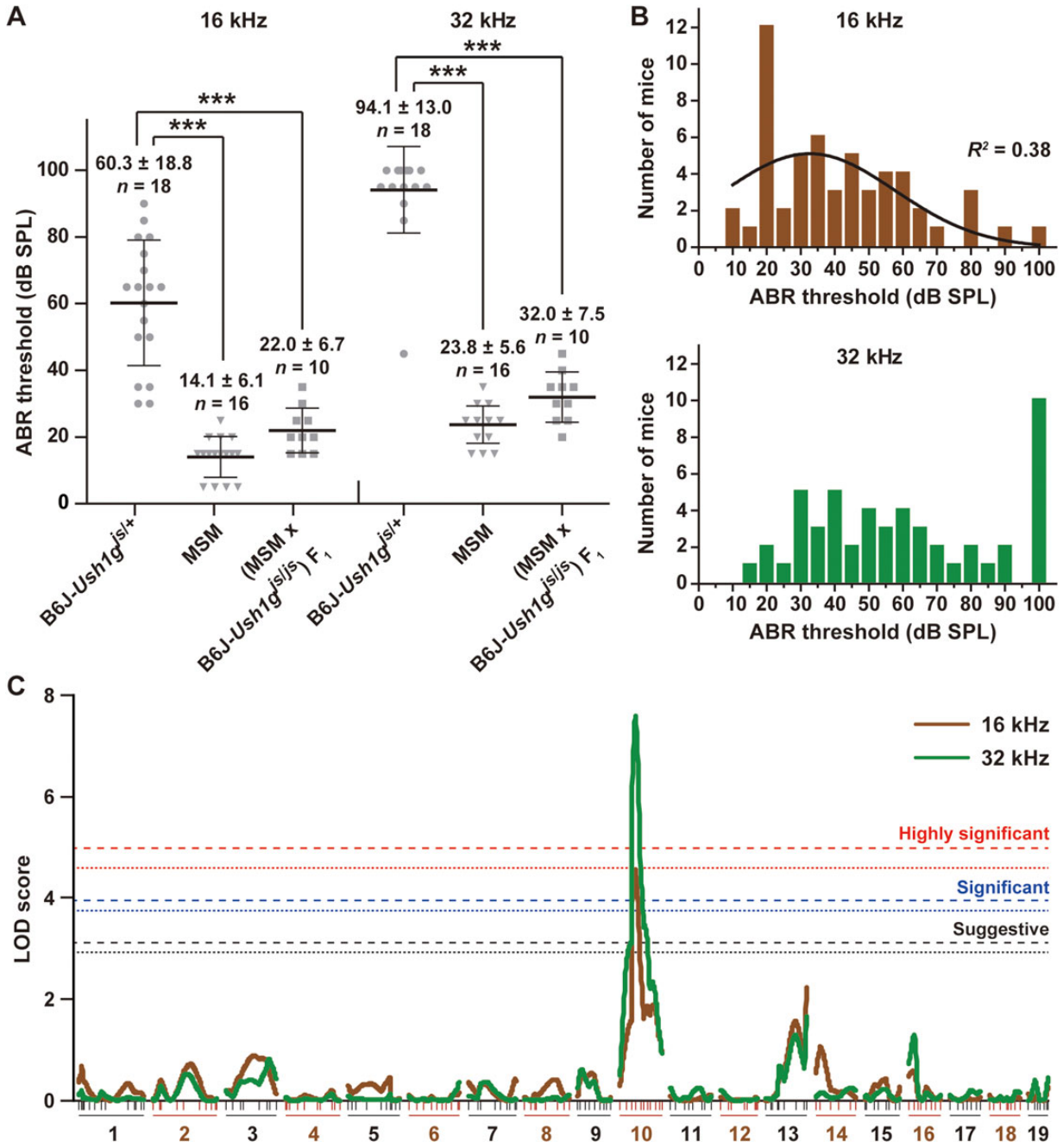

Figure 2. Genetic analysis of the susceptibility gene associated with ePHL of B6J-*Ush1g*$^{js/+}$ heterozygous mice. (**A**) The means (middle bold lines) and SDs (error bars) of ABR threshold measurements for 16 and 32 kHz stimuli in B6J-*Ush1g*$^{js/+}$, MSM and (MSM × B6J-*Ush1g*$^{js/js}$) F_1 mice at 4 months of age. The dots represent the ABR thresholds of individual mice. ***$P < 0.001$. (**B**) Distributions of ABR thresholds for 16 (top, brown bars) and 32 (bottom, green bars) kHz stimuli among the (MSM × B6J-*Ush1g*$^{js/js}$) F_1 × B6J-*Ush1g*$^{js/js}$ backcrossed (N_2) mice of the *Ush1g*$^{js/+}$ heterozygous genotype. The best-fit curves for a Gaussian distribution are shown in black. The regression coefficient for the curve is given as R^2 and was calculated using the D'Agostino and Pearson test. (**C**) Genome-wide interval mapping for the susceptibility gene associated with ePHL for 16 (brown curve) and 32 (green curve) kHz stimuli of the N_2-*Ush1g*$^{js/+}$ heterozygous mice. Chromosome numbers and marker positions (vertical bars) are given beneath the linkage maps. The horizontal dotted (16 kHz) and dashed (32 kHz) lines indicate suggestive (black, $P < 0.05$, LOD score = 16 kHz: 2.92 and 32 kHz: 3.11), significant (blue, $P < 0.01$, LOD = 16 kHz: 3.74 and 32 kHz: 3.94) and highly significant (red, $P < 0.001$, LOD = 16 kHz: 4.58 and 32 kHz: 4.97) linkage associations.

(MSM × B6J-*Ush1g*$^{js/js}$) F_1 mice. Likewise, thresholds at 32 kHz in the backcross progeny were divided into two groups at a ratio of 1:1.2 according to the mean (54.4 dB SPL) thresholds from the *Ush1g*$^{js/+}$, MSM and F_1 mice, thus suggesting that the *Ush1g*$^{js/+}$ heterozygous mice developed ePHL because of the effect of a single locus.

To define the susceptibility locus underlying the ePHL of *Ush1g*$^{js/+}$ heterozygous mice, we performed genome-wide QTL linkage mapping. A QTL linkage analysis of the progeny ($n = 51$) of the *Ush1g*$^{js/+}$ heterozygous genotype selected from [(MSM × B6J-*Ush1g*$^{js/js}$) F_1 × B6J-*Ush1g*$^{js/js}$] N_2 mice revealed a highly significant linkage association on chromosome 10 to the ABR thresholds at both 16 and 32 kHz at 4 months of age, with a peak at marker *D10Mit138* (LOD = 4.56 at 16 kHz and LOD = 7.59 at 32 kHz; Fig. 2C). Although we detected a linkage association with the distal region of chromosome 13, the peak LODs showed a nearly suggestive linkage at *D13Mit35* (LOD = 2.24 at 16 kHz and LOD = 1.67 at 32 kHz; Fig. 2C).

To confirm the effect of the susceptibility locus on chromosome 10 on the ABR thresholds in *Ush1g*$^{js/+}$ mice, we analyzed the B6J-*Ush1g*$^{js/+}$, -Chr10^{MSM} congenic mice by crossing (B6J × B6J-Chr10$^{MSM/MSM}$ consomic mice) F_1 × B6J-*Ush1g*$^{js/js}$ mice (Supplementary Material, Fig. S3). We produced seven B6J-Chr10$^{B6J/B6J}$ homozygous, 20 B6J-Chr10$^{B6J/MSM}$ heterozygous and 78 B6J-Chr10^{MSM} congenic mice from the *Ush1g*$^{js/+}$ genotype through this mating. The ABR thresholds at 16 and 32 kHz at 4 months of age were significantly different between the B6J-*Ush1g*$^{js/+}$, -Chr10$^{B6J/B6J}$ and -Chr10$^{B6J/MSM}$ mice (Fig. 3 and Supplementary Material, Table S2, $P < 0.001$); therefore, we confirmed the existence of a susceptibility locus on chromosome 10 in the cross by using a B6J-Chr10$^{MSM/MSM}$ consomic strain. The B6J-*Ush1g*$^{js/+}$,

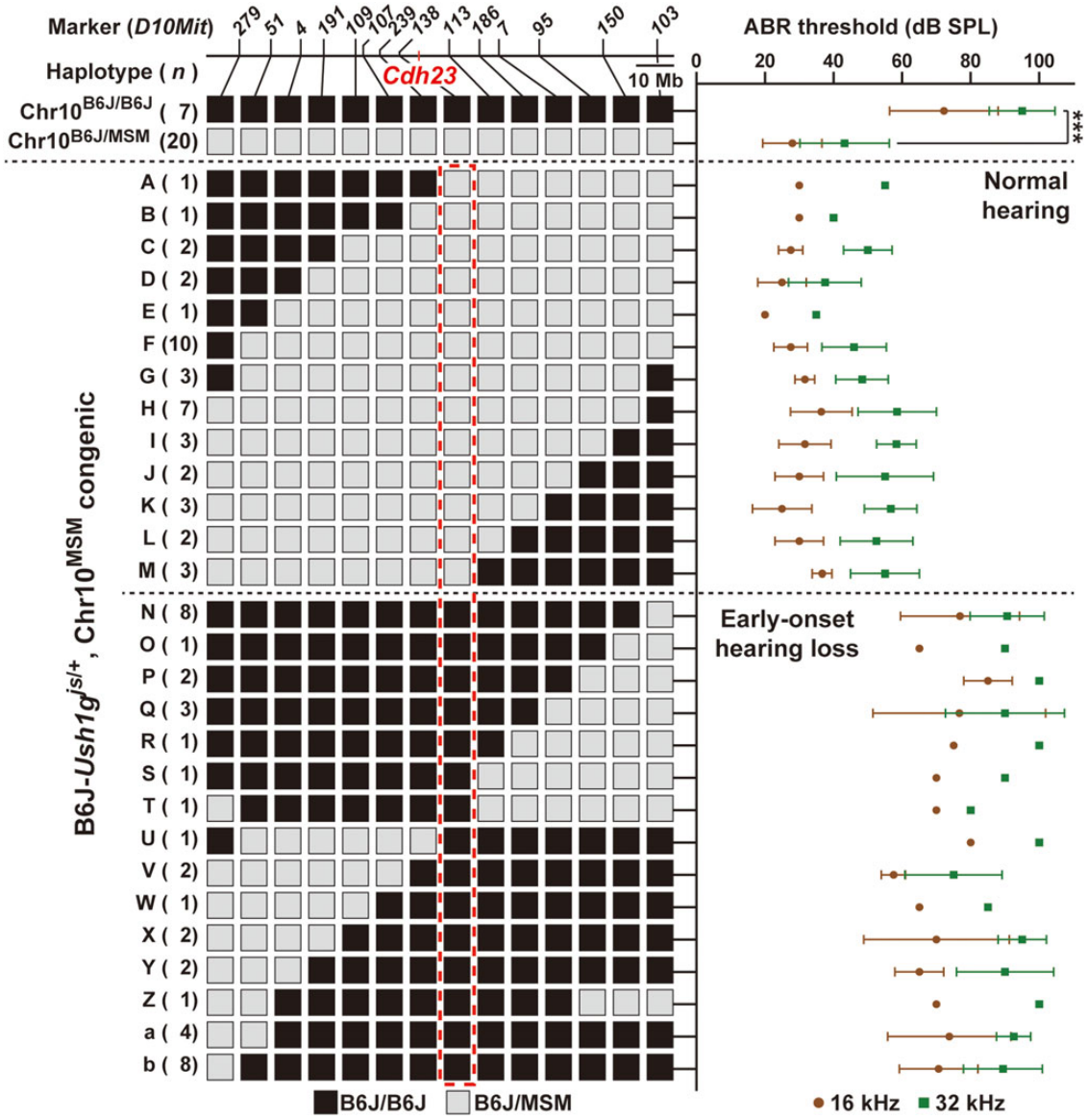

Figure 3. Genetic analysis of the susceptibility gene associated with ePHL of B6J-*Ush1g*$^{js/+}$, -Chr10^{MSM} congenic mice produced by cross of (B6J × B6J-Chr10$^{MSM/MSM}$ consomic mice) F_1 × B6J-*Ush1g*$^{js/js}$ mice. The left panel shows the haplotypes of Chr10 in B6J-*Ush1g*$^{js/+}$, -Chr10$^{B6J/B6J}$ ($n = 7$), -Chr10$^{B6J/MSM}$ ($n = 20$) and -Chr10^{MSM} congenic ($n = 78$) mice. The positions of the genetic markers and *Cdh23* are indicated above the haplotype map. The red dashed box indicates genotypes of congenic mice in *D10Mit138*, which was non-recombinant with hearing phenotypes. The right graph indicates the means (circles and squares) and SDs (error bars) of the ABR threshold measurements for 16 (brown) and 32 (green) kHz stimuli in B6J-*Ush1g*$^{js/+}$, -Chr10$^{B6J/B6J}$, -Chr10$^{B6J/MSM}$ and -Chr10^{MSM} congenic mice at 4 months of age. ***$P < 0.001$.

-Chr10^{MSM} congenic mice were clearly classified into two distinct hearing groups consisting of normal hearing (mean thresholds: 30.3 ± 7.0 dB SPL at 16 kHz and 51.1 ± 10.5 dB SPL at 32 kHz) and ePHL (72.5 ± 13.9 dB SPL at 16 kHz and 90.7 ± 10.4 dB SPL at 32 kHz) according to the B6J/MSM heterozygous and B6J/B6J homozygous genotypes of *D10Mit138* (Chr 10: 53 772 094–53 772 211), respectively (Fig. 3). *Cdh23*, a gene known to be causative for hearing impairments in humans (1,2,20) and mice (12,15,40), is located in the distal region (Chr 10: 60 302 748–60 696 490), ~6.5 Mb from the non-recombinant marker *D10Mit138* (Fig. 3).

Elucidation of an epistatic effect between the *Ush1g* and *Cdh23* mutant alleles on ePHL

Previous studies have reported that the age-related hearing loss (*ahl*) mutation (*Cdh23*^{ahl}, c.753G>A) in *Cdh23* is responsible for age-related hearing loss (AHL) in multiple inbred mouse strains, including B6J mice (15,40–45). Therefore, we hypothesized that epistasis (the interaction of multiple genes to determine a phenotype (46)) between the *Ush1g*^{js} and *Cdh23*^{ahl} alleles would affect the development of ePHL in *Ush1g*$^{js/+}$ heterozygous mice with a B6J genetic background. To confirm the hypothesis, we used forward and reverse genetic approaches.

First, we investigated the hearing level of high-frequency sounds of F_1 mice of the B6J-*Ush1g*$^{+/+}$/B6J-*Ush1g*$^{js/js}$ genotype and two other strains carrying the *Cdh23*^{ahl} allele to define the epistasis between the *Ush1g*^{js} and *Cdh23*^{ahl} alleles on ePHL in different genetic backgrounds. We crossed B6J-*Ush1g*$^{+/+}$ and -*Ush1g*$^{js/js}$ mice to yield DBA/2J (D2J) mice, which developed ePHL with additive and/or interactive epistatic effects between the *Cdh23*^{ahl} and *ahl8* mutations (rs26996001G>A, p.Arg109His) in the fascin 2 gene (*Fscn2*) (42,44,47,48). We also measured the ABR thresholds at 16 and 32 kHz stimuli at 4 months of age. The ABR thresholds at 32 kHz were significantly different between (D2J × B6J) F_1-*Ush1g*$^{+/+}$ and -*Ush1g*$^{js/+}$ mice, although (D2J × B6J) F_1 mice already had developed severe hearing loss at this stage from the effect of another dominant modifier gene(s), as suggested by our previous study (Fig. 4) (44). We showed that the average ABR threshold at 16 kHz was significantly higher in (D2J × B6J) F_1-*Ush1g*$^{js/+}$ mice, at 37.3 dB SPL ($P < 0.001$), than in (D2J × B6J) F_1-*Ush1g*$^{+/+}$ mice (Fig. 4). Moreover, the effects of the *Ush1g*^{js} allele on hearing loss were observed in F_1 mice from B6J and A/J mice, which developed ePHL, and these mice may exhibit additive effects of the *Cdh23*^{ahl}, *ahl4* mutation (rs29358506C>A, p.55His>Asn) in citrate synthase (*Cs*) and a single adenine insertion in the mitochondrial tRNA-Arg gene (*mt-Tr*^{Arg}) (Fig. 4) (45,49). In (A/J × B6J) F_1-*Ush1g*$^{js/+}$ mice, the average ABR thresholds at both 16 and 32 kHz were higher, at 16.9 ($P < 0.05$) and 23.3 dB SPL ($P < 0.001$), respectively, than those of the (A/J × B6J) F_1-*Ush1g*$^{+/+}$ mice (Fig. 4). We estimated that there were no effects from the single *Cs*^{ahl4} allele or the maternally transmitted adenine insertion in *mt-Tr*^{Arg} on hearing ability following phenotypic observation of (A/J × B6J) F_1-*Ush1g*$^{+/+}$ mice. Thus, our results showed that the combination of the single *Ush1g*^{js} allele and homozygosity of the *Cdh23*^{ahl} allele resulted in the development of ePHL in another genetic background.

Next, we produced *Cdh23*$^{c.753A>G}$ KI mice and obtained B6J-*Ush1g*$^{js/+}$, *Cdh23*$^{c.753A/G}$ double-heterozygous mice to define the epistasis between the *Ush1g*^{js} and *Cdh23*^{ahl} alleles. We performed genome editing using the CRISPR/Cas9 system and designed a Cas9/gRNA target sequence in the vicinity of the *Cdh23*$^{c.753}$ site in the B6J genomic sequence (Supplementary Material, Fig. S4A). The Cas9 mRNA, *Cdh23*-sgRNA and donor oligonucleotide were designed to include c.753A>G with a synonymous c.714C>T substitution to avoid cleavage by Cas9 and to provide evidence of an artificial KI (Supplementary Material, Fig. S4A

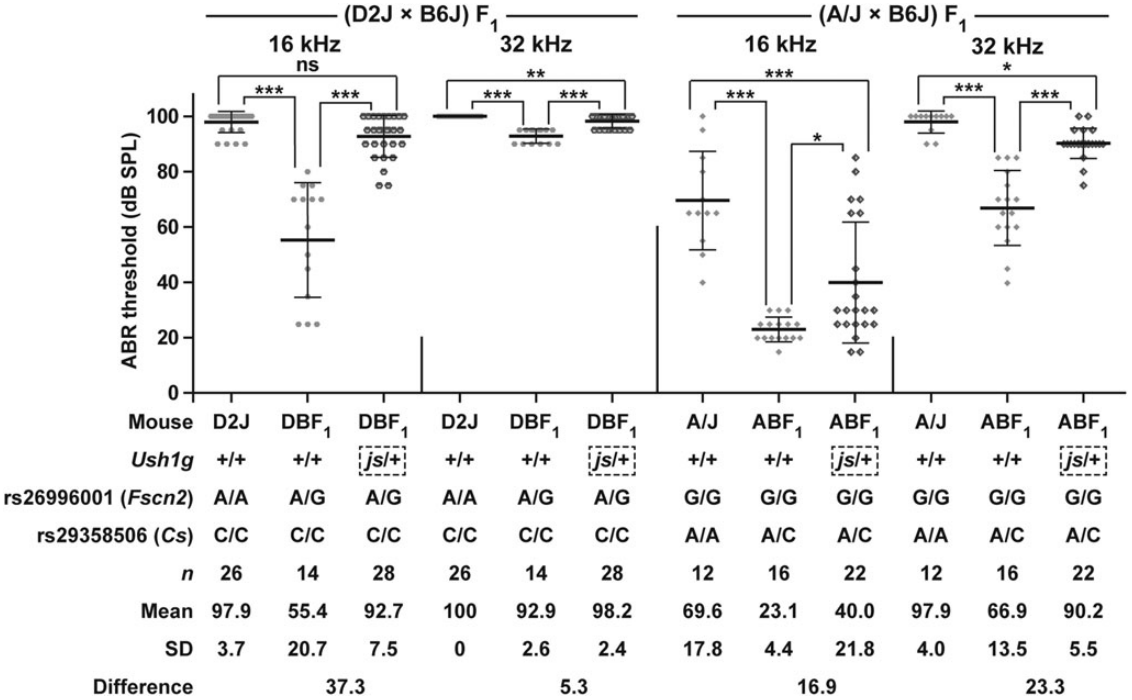

Mouse	D2J	DBF$_1$	DBF$_1$	D2J	DBF$_1$	DBF$_1$	A/J	ABF$_1$	ABF$_1$	A/J	ABF$_1$	ABF$_1$
Ush1g	+/+	+/+	*js*/+	+/+	+/+	*js*/+	+/+	+/+	*js*/+	+/+	+/+	*js*/+
rs26996001 (*Fscn2*)	A/A	A/G	A/G	A/A	A/G	A/G	G/G	G/G	G/G	G/G	G/G	G/G
rs29358506 (*Cs*)	C/C	C/C	C/C	C/C	C/C	C/C	A/A	A/C	A/C	A/A	A/C	A/C
n	26	14	28	26	14	28	12	16	22	12	16	22
Mean	97.9	55.4	92.7	100	92.9	98.2	69.6	23.1	40.0	97.9	66.9	90.2
SD	3.7	20.7	7.5	0	2.6	2.4	17.8	4.4	21.8	4.0	13.5	5.5
Difference		37.3			5.3			16.9			23.3	

Figure 4. Effects of the *Ush1g*^{js} allele on ePHL in the (D2J × B6J) F_1 and (A/J × B6J) F_1 mice. The means (middle bold lines), SDs (error bars) and phenotypes (dots) of individual mice of the ABR thresholds at 16 and 32 kHz are shown for each *Ush1g*$^{+/+}$ and *Ush1g*$^{js/+}$ genotype at 4 months of age. The data for ABR threshold measurements in D2J mice are cited from our previous study (44). Differences between the means of mice of *Ush1g*$^{+/+}$ and *Ush1g*$^{js/+}$ genotypes in each F_1 mouse are shown. In the *Fscn2* locus: G, wild-type allele; A, *ahl8* mutant allele. In the *Cs* locus: C, wild-type allele; A, *ahl4* mutant allele. ns, no significant difference; *$P < 0.05$, **$P < 0.01$ and ***$P < 0.001$.

and Table S3). We produced a B6J-*Cdh23*$^{c.753A/G}$ KI mouse by co-injection of the Cas9 mRNA, *Cdh23*-sgRNA and donor oligonucleotide into the pronuclei and cytoplasm of fertilized mouse eggs and performed screening using mutation analyses (Fig. 5A) (see the Materials and Methods section and Supplementary Material, Figs S4 and S5 for details). In this KI mouse, the sequencing of 10 potential off-target sequences revealed no off-target effects in any of the mice derived from Cas9 and Cas9-nickase targeting (Supplementary Material, Table S4). A B6J-*Cdh23*$^{c.753A/G}$ KI mouse was crossed once with B6J mice, and then homozygous *Cdh23*$^{c.753G/G}$ KI mice were produced by sibling mating (Supplementary Material, Fig. S4C). We confirmed that both the c.714T and c.753G substitutions were inherited without segregation in all the progeny of the KI mice by using sequencing. The *Cdh23*$^{c.753G>A}$ mutation is located at a splice junction (Fig. 5A and Supplementary Material, Fig. S4A), thus altering the consensus splice donor site and leading to the in-frame skipping of exon 7 of *Cdh23* in B6J mice (15,40). We performed an RT-PCR analysis to examine whether the skipping of exon 7 was abrogated in B6J-*Cdh23*$^{c.753A>G}$ KI mice. The in-frame skipping of exon 7 and partial alternative splicing was detected in B6J mice by RT-PCR with primers located on exons 6 and 8 (Supplementary Material,

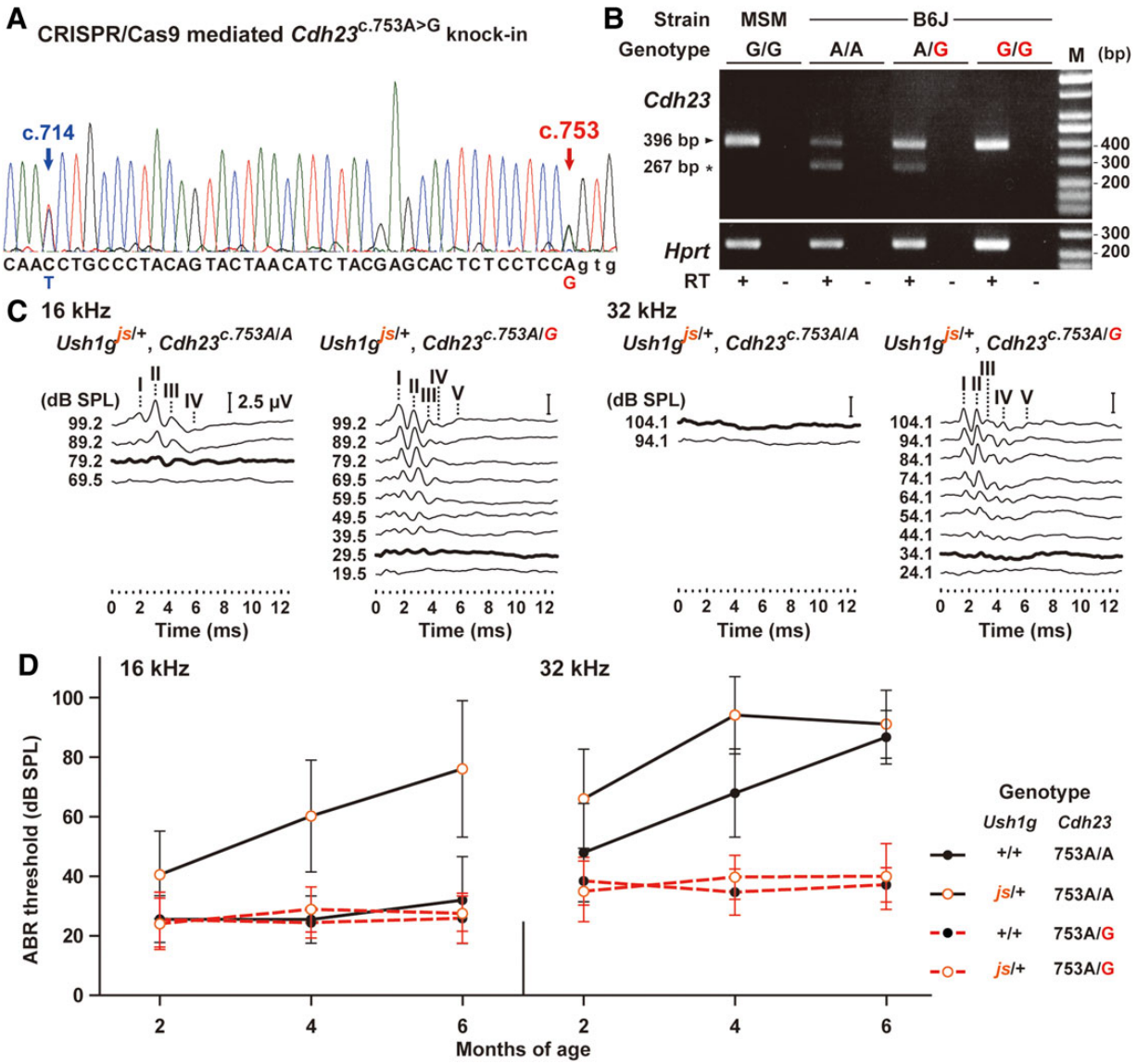

Figure 5. Targeted *Cdh23*$^{c.753A>G}$ KI in the B6J mice using CRISPR/Cas9 genome editing and rescue of the ePHL in B6J-*Ush1g*$^{js/+}$ mice. (**A**) A sequence of the targeted region in *Cdh23* from a F_0 offspring (No. 33) produced by co-injection of the Cas9 mRNA, *Cdh23*-sgRNA and donor oligonucleotide (Supplementary Material, Fig. S4A and Table S3). The C/T and A/G hetero peaks were detected in synonymous c.714 (blue arrow) and c.753 (red arrow) sites, respectively. (**B**) Rescue of partial alternative splicing of exon 7 of *Cdh23* in B6J mice by Cas9-mediated KI. The upper panel shows the electrophoretic profile of RT-PCR products amplified from cochlear cDNA from *Cdh23*^{753G} (MSM and B6J-*Cdh23*$^{c.753G/G}$) and *Cdh23*^{753A} (B6J) homozygous mice and B6J-*Cdh23*$^{c.753A/G}$ heterozygous mice using *Cdh23*-specific primers located in exons 6 and 8 (Supplementary Material, Table S3). The 396 and 267 bp bands indicate spliced in and out exon 7, respectively. cDNA integrity was confirmed using a hypoxanthine-guanine phosphoribosyl transferase (*Hprt*) control band (bottom panel). M: marker (100-bp DNA ladder). (**C**) Representative ABR waveforms from B6J-*Ush1g*$^{js/+}$, -*Cdh23*$^{c.753A/A}$ and -*Ush1g*$^{js/+}$, -*Cdh23*$^{c.753A/G}$ mice at 4 months of age. The waveforms represent the ABR in response to tone-pip stimuli at 16 (left) and 32 (right) kHz. The bold lines represent the thresholds detected. The locations of Peaks I–V are indicated. Scale bars = 2.5 µV. (**D**) The means (circles) and SDs (error bars) of ABR threshold measurements for 16 and 32 kHz stimuli are shown for B6J mice of four different combinations in *Ush1g* and *Cdh23* genotypes at 2, 4 and 6 months of age.

Table S3). In B6J-*Cdh23*$^{c.753A/G}$ heterozygous mice, the smaller PCR fragment (267 bp), which indicates that exon 7 was skipped, was detectable as a faint signal. However, the expression level of the unspliced fragment (396 bp) was markedly increased relative to that of the B6J-*Cdh23*$^{c.753A/A}$ mice (Fig. 5B). Moreover, the smaller 267 bp fragment was not detectable in the B6J-*Cdh23*$^{c.753G/G}$ homozygous mice, and the expression level was similar to that of the *Cdh23*$^{c.753G/G}$ MSM mice (Fig. 5B). We determined the ABR thresholds for sound stimuli at 4, 8, 16 and 32 kHz in B6J-*Cdh23*$^{c.753A/G}$ mice at 1–12 months of age at 1-month intervals. The B6J-*Cdh23*$^{c.753A/G}$ mice did not develop AHL up to 12 months of age (Supplementary Material, Fig. S6 and Table S5). We subsequently produced B6J-*Ush1g*$^{js/+}$, *Cdh23*$^{c.753A/G}$ double-heterozygous mice by mating B6J-*Ush1g*$^{js/js}$ and -*Cdh23*$^{c.753G/G}$ mice and evaluated their hearing levels of high-frequency sound stimuli. Figure 5C shows representative ABR waveforms at 16 and 32 kHz stimuli for mice at 4 months of age. B6J-*Ush1g*$^{js/+}$, *Cdh23*$^{c.753A/A}$ mice exhibited latency peak responses for peaks I–IV at 16 kHz, but the amplitudes of all the peaks were weak (Fig. 5C). At 32 kHz, the peak responses were undetectable even at the maximum dB SPL. By contrast, B6J-*Ush1g*$^{js/+}$, *Cdh23*$^{c.753A/G}$ mice exhibited acute peak responses for peaks I–V at both 16 and 32 kHz (Fig. 5C). We determined the age dependency of ABR thresholds for tone-pip stimuli at 16 and 32 kHz in mice at 2, 4, and 6 months of age. At 16 kHz, B6J-*Ush1g*$^{js/+}$, *Cdh23*$^{c.753A/G}$ and B6J-*Ush1g*$^{+/+}$, *Cdh23*$^{c.753A/G}$ mice exhibited ABR thresholds significantly lower than those of B6J-*Ush1g*$^{js/+}$, *Cdh23*$^{c.753A/A}$ mice, and differences in age did not affect the ABR thresholds (Fig. 5D and Supplementary Material, Fig. S6). At 32 kHz, in contrast, B6J-*Ush1g*$^{js/+}$, *Cdh23*$^{c.753A/G}$ mice and B6J-*Ush1g*$^{+/+}$, *Cdh23*$^{c.753A/G}$ mice maintained their hearing levels for the stimulus, and an age-dependent effect was not observed; however, B6J-*Ush1g*$^{js/+}$, *Cdh23*$^{c.753A/A}$ mice and B6J mice with the *Cdh23*$^{c.753A/A}$ genotype developed progressive hearing loss (PHL) (Fig. 5D and Supplementary Material, Fig. S7). These results showed that the *Cdh23*$^{c.753A>G}$ substitution completely rescued the ePHL in B6J-*Ush1g*$^{js/+}$ heterozygous mice. This result strongly suggests the presence of epistasis between the *Ush1g*^{js} and *Cdh23*$^{c.753A}$ alleles, which leads to the ePHL in B6J-*Ush1g*$^{js/+}$ mice.

Age-related degeneration of stereocilia in hair cells inside the organ of Corti in *Ush1g*$^{js/+}$ heterozygous mice and phenotype rescue by *Cdh23*$^{c.753A>G}$ knock-in

Previous studies have reported that the degeneration of hair cells in the organ of Corti (oC) correlates with PHL in mice (4,15,47,48,50). In addition, *Ush1g*- and *Cdh23*-mutant mice display similar stereocilia degeneration (8,12–15). We therefore used scanning electron microscopy (SEM) to observe the age-related phenotypes of the stereocilia on oC hair cells in B6J-*Ush1g*$^{js/+}$ (*Cdh23*$^{c.753A/A}$ homozygous) heterozygous mice. Although we did not observe severe defects in the phenotype of the stereocilia on the inner hair cells (IHCs) in B6J-*Ush1g*$^{js/js}$ homozygous mutants at 1 month of age (Fig. 6A), the stereocilia on the OHCs were severely degenerated as previously reported (Fig. 6B) (13,14). By contrast, in B6J-*Ush1g*$^{js/+}$ heterozygous mice, the stereocilia displayed normal morphologies, with strictly organized 'V'-shaped and staircase-like configurations on OHCs (Fig. 6C and D) and crescent- and staircase-shaped configurations on IHCs (Fig. 6C). However, we found that a few stereocilia on OHCs at the base of the oC were missing and disrupted (Fig. 6E and F). Moreover, the stereocilia in B6J-*Ush1g*$^{js/+}$ mice showed progressive degeneration in other areas of the oC with increasing age. At 3 months of age, the stereocilia were defective in most OHCs inside the middle region of the cochlea, and several in the shortest row had been lost (Fig. 6G and H). Additionally, we found elongated stereocilial links on the stereocilia of OHCs in B6J-*Ush1g*$^{js/+}$ heterozygous mice at 3 months of age (Fig. 6G and I). By 6 months of age, the degree of OHC degeneration in B6J-*Ush1g*$^{js/+}$ mice was higher than it was at 3 months of age (Fig. 6G–I), and phenotypes of the stereocilia were notably different from that of the virtually normal stereocilia (Supplementary Material, Fig. S8A) in B6J-*Ush1g*$^{+/+}$ mice at the same age. The phenotypes of OHCs in B6J-*Ush1g*$^{js/+}$ mice were characterized by missing and shortened stereocilia in the shortest row (Fig. 6J). Although the stereocilia were degenerated in the OHCs of B6J-*Ush1g*$^{+/+}$ mice at 10 months of age (Supplementary Material, Fig. S8B), the stereocilia degeneration in B6J-*Ush1g*$^{js/+}$ mice became even more severe in comparison with the phenotypes of the B6J-*Ush1g*$^{+/+}$ mice (Fig. 6K). The OHC stereocilia were mostly disrupted in B6J-*Ush1g*$^{js/+}$ heterozygous mice at 10 months of age (Fig. 6K). We found missing stereocilia on OHCs (Fig. 6K), and the shortest row was completely lost in surviving OHCs (Fig. 6L). By contrast, the IHC phenotype was mostly normal in B6J-*Ush1g*$^{js/+}$ mice (Fig. 6M).

Next, we compared the hair cells from the apical (area 1) and middle (area 2) turns (Supplementary Material, Fig. S9) of the oC in B6J-*Ush1g*$^{js/+}$ heterozygous mice with those from B6J-*Ush1g*$^{js/js}$ homozygous and -*Ush1g*$^{+/+}$ mice because the cochlear hair cells showed rapid degeneration in mutant *Ush1g* mice (13). We first noticed that the hair cells showed rapid degeneration in both the apical and middle turns in B6J-*Ush1g*$^{js/js}$ homozygous mice compared with B6J-*Ush1g*$^{js/+}$ heterozygous and -*Ush1g*$^{+/+}$ mice (Fig. 7A). Losses of approximately 33 and 38% of OHCs were observed at the apical and middle turns, respectively, in B6J-*Ush1g*$^{js/js}$ mice at 3 months of age. By 6 months of age, only a few OHCs were present in both the apical and middle turns. Although the loss of IHCs reached 20–30% in both areas at this age, the IHC loss was lower than that observed for OHCs (Fig. 7A). However, we did not detect a distinct loss of hair cells in B6J-*Ush1g*$^{js/+}$ heterozygous mice at 1 and 3 months of age, and no difference in either OHCs or IHCs was observed between B6J-*Ush1g*$^{js/+}$ and -*Ush1g*$^{+/+}$ mice. However, different degrees of OHC degeneration were observed in the apical and middle turns by 6 months of age, and approximately 15% of the OHCs in both areas were lost in B6J-*Ush1g*$^{js/+}$ mice (Fig. 7B). After 6 months of age, the OHCs were gradually lost in the middle turn. The OHCs in the middle turn at 9 and 12 months of age were reduced to approximately 74 and 54%, respectively, of the numbers present at 6 months of age (Fig. 7B). Although a significant loss of OHCs was observed in the middle area of B6J-*Ush1g*$^{+/+}$ mice (Fig. 7C), the hair cell loss was more severe in B6J-*Ush1g*$^{js/+}$ mice (Fig. 7B). In addition, hair cell loss was observed mostly in OHCs but was not obvious in IHCs. We also investigated the phenotypes of the hair cells and stereocilia in C3H-*Ush1g*$^{seal/+}$ mice. There was no hair cell loss in C3H-*Ush1g*$^{seal/+}$ mice up to 12 months of age (Supplementary Material, Fig. S10A), and the gross morphology of stereocilia was not affected in C3H-*Ush1g*$^{seal/+}$ mice (Supplementary Material, Fig. S10C) in comparison with C3H-*Ush1g*$^{+/+}$ mice (Supplementary Material, Fig. S10B).

The progressive degeneration and lack of stereocilia and OHCs in B6J-*Ush1g*$^{js/+}$ heterozygous mice was completely rescued by the *Cdh23*$^{c.753A>G}$ KI. At 6 months of age, the stereocilia of B6J-*Ush1g*$^{js/+}$, -*Cdh23*$^{c.753A/G}$ mice were organized into 'V'-shaped and staircase-like configurations on the OHCs (Fig. 8A and B), which were similar to those of B6J-*Ush1g*$^{+/+}$, *Cdh23*$^{c.753A/A}$ mice (Fig. 8C), and they did not show any loss or shortening as found in B6J-*Ush1g*$^{js/+}$, *Cdh23*$^{c.753A/A}$ mice (Fig. 8D). Moreover, the

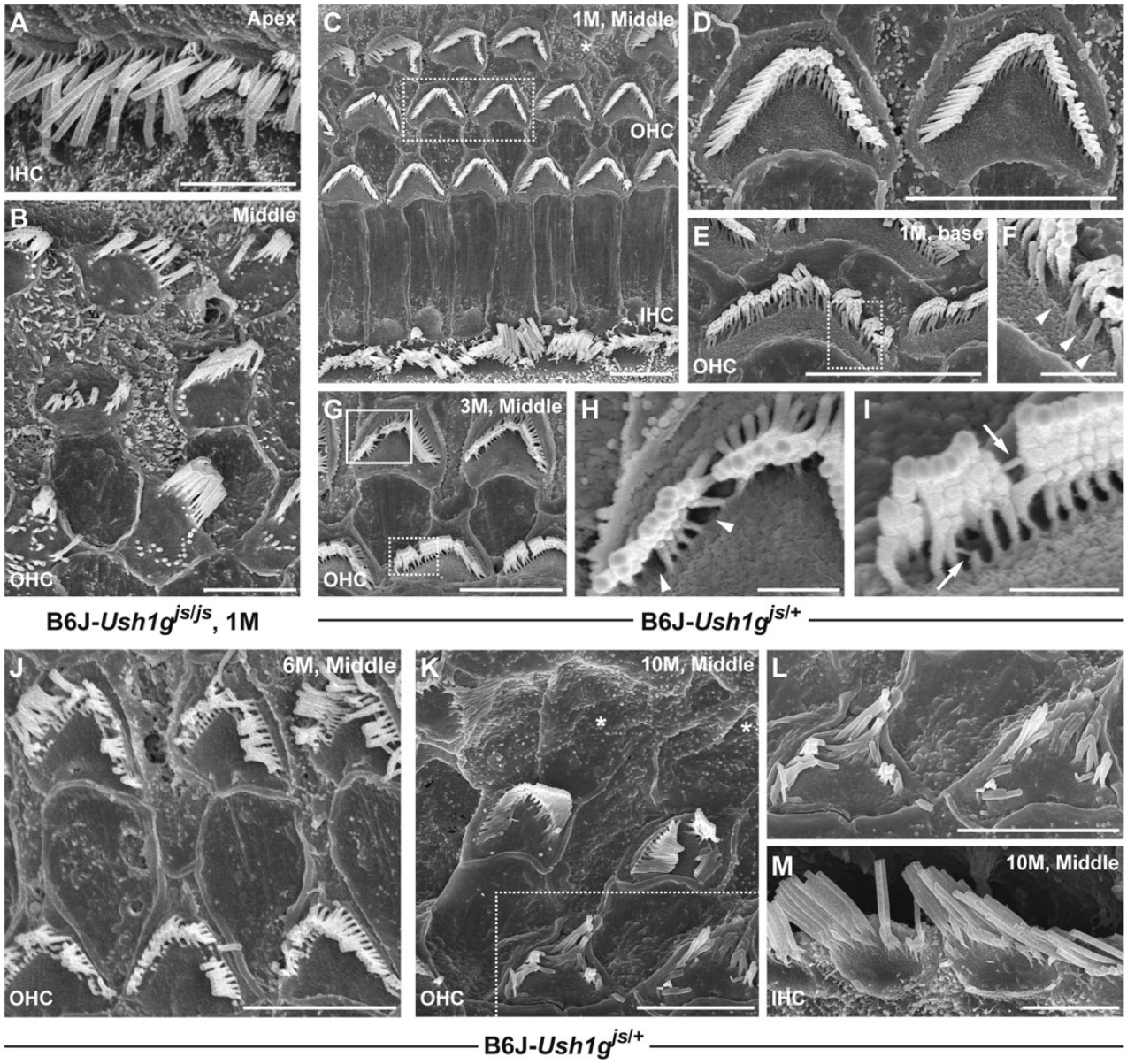

Figure 6. SEM images showing the stereocilia of the hair cells from the organ of Corti in B6J-*Ush1g*$^{js/js}$ homozygous and -*Ush1g*$^{js/+}$ heterozygous mice. (**A** and **B**) Stereociliary morphology of the IHCs (A) and OHCs (B) from the apex (A) and middle (B) areas in B6J-*Ush1g*$^{js/js}$ mice at 1 month of age (1 M). (**C–F**) Stereociliary morphology of the hair cells from the middle (C and D) and base (E and F) areas of the organ of Corti in B6J-*Ush1g*$^{js/+}$ mice at 1 M. The asterisks indicate OHCs with absent bundles. Highly magnified images of the stereocilia in the dotted boxes in C and E are shown in D and F, respectively. (**G–I**) Stereociliary phenotypes of the OHCs (middle area) in B6J-*Ush1g*$^{js/+}$ mice at 3 M. Highly magnified images of the stereocilia in the solid box and dotted box in G are shown in H and I, respectively. The arrowheads (F and H) indicate the absence of stereocilia, and the arrows (I) indicate the elongated stereociliary links. (**J–M**) Age-related degeneration of stereocilia on cochlear hair cells in B6J-*Ush1g*$^{js/+}$ heterozygous mice. Stereociliary phenotypes of OHCs (J–L) and IHCs (M) from the middle area of the organ of Corti in B6J-*Ush1g*$^{js/+}$ mice at 6 (6M, J) and 10 months of age (10M, K–M). Scale bars = 5 μm (A–E, G and J–M) and 2 μm (F, H and I).

missing OHCs were not detected until at least 6 months of age in B6J-*Ush1g*$^{js/+}$, -*Cdh23*$^{c.753A/G}$ mice (Supplementary Material, Fig. S11A and B).

Discussion

In this study, we showed that *Ush1g*$^{js/+}$ heterozygous mice developed ePHL (Fig. 1 and Supplementary Material, Table S1), which began in the high-frequency region and spread toward the low frequencies with aging; this pattern is consistent with the common clinical features of DFNA patients (34,35). Furthermore, we demonstrated that ePHL in *Ush1g*$^{js/+}$ mice was affected by the *Cdh23*^{ahl} locus found in most laboratory strains, including B6J, A/J, and D2J mice, but not in C3H or MSM mice (Figs 2–5). This background effect was determined by a linkage analysis in backcrossed mice (Fig. 2) and Chr10^{MSM} congenic mice (Fig. 3 and Supplementary Material, Table S2). Analysis of A/J and D2J mice confirmed the effect of the *Cdh23*^{ahl} locus and suggested that genetic modifiers other than *Cdh23*^{ahl} exist for ePHL (Fig. 4). More importantly, the *Cdh23*^{ahl} effect was directly determined by c.753A>G editing of the *Cdh23*^{ahl} mutation (Fig. 5A and B). The *Cdh23*$^{c.753A>G}$ substitution resulted in complete recovery from ePHL in B6J-*Ush1g*$^{js/+}$ heterozygous mice (Fig. 5C and D). These results showed that ePHL developed through the additive effect of

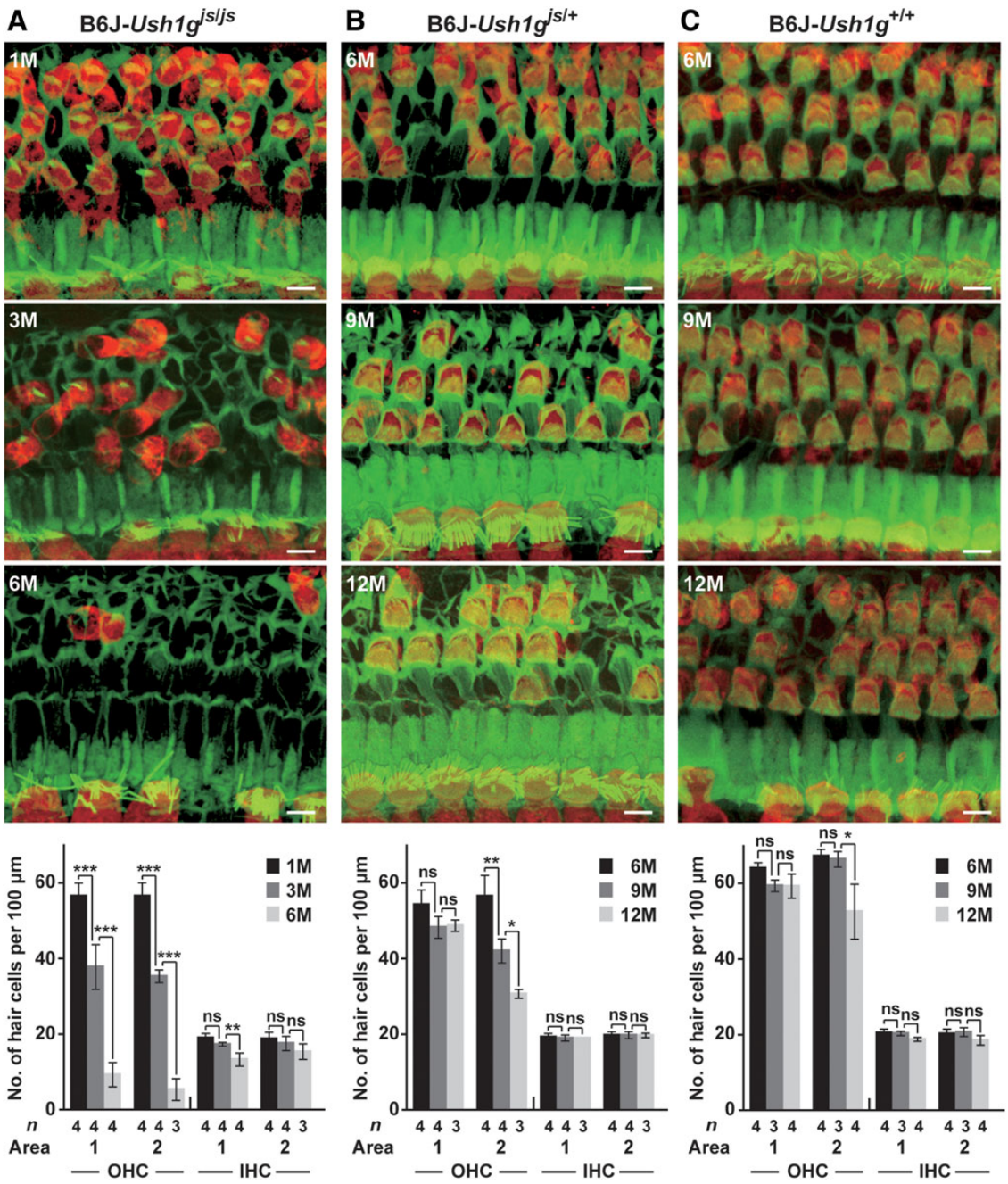

Figure 7. Defect of OHCs in B6J-*Ush1g*$^{js/+}$ heterozygous mice. (**A**) Confocal images (first to third panels from the top) of the hair cells and the counts (bottom) of the hair cells in Areas 1 and 2 (1.2–1.5 and 2.1–2.4 mm from the apex, see Supplementary Material, Fig. S9) in the organ of Corti of B6J-*Ush1g*$^{js/js}$ homozygous mice. The images show hair cells from Area 2 visualized by immunohistochemistry of phalloidin (green) and anti-MYO6 antibody (red) in mice at 1 (1st), 3 (2nd) and 6 (3rd) months of age. (**B** and **C**) Confocal images of hair cells and counts (bottom) of the hair cells from Areas 1 and 2 in the organ of Corti of B6J-*Ush1g*$^{js/+}$ (B) and -*Ush1g*$^{+/+}$ (C) mice at 6 (1st), 9 (2nd) and 12 (3rd) months of age. Scale bars = 5 µm.

one dominant *Ush1g*^{js} allele and homozygous alleles of *Cdh23*$^{c.753A}$.

As described in the Introduction, the majority of human cases of PHL are caused by a dominant mutation whose penetrance is lower than that in homozygotes with recessive mutations (34–36). This finding suggests that a single mutant allele alone does not have a strong effect on the development of hearing loss. In a previous study, Vona *et al.* (37) have shown that potentially damaging variants of deafness genes accumulate in patients diagnosed with dominant NSHL caused by pathogenic heterozygous mutations compared with normal-hearing controls and patients diagnosed with recessive NSHL. Moreover, Vona *et al.* (37) indicated that NSHL patients undiagnosed by mutation screening have significantly more damaging variants of deafness genes than normal-hearing controls, suggesting that NSHL is caused by an accumulation of unfavorable variants across potentially multiple genes associated with hearing loss. In addition, the expression of the phenotype by double-heterozygous mutations in two deafness causative genes, i.e. digenic inheritance, has been reported in patients with NSHL (51) and NSHL associated with enlarged vestibular

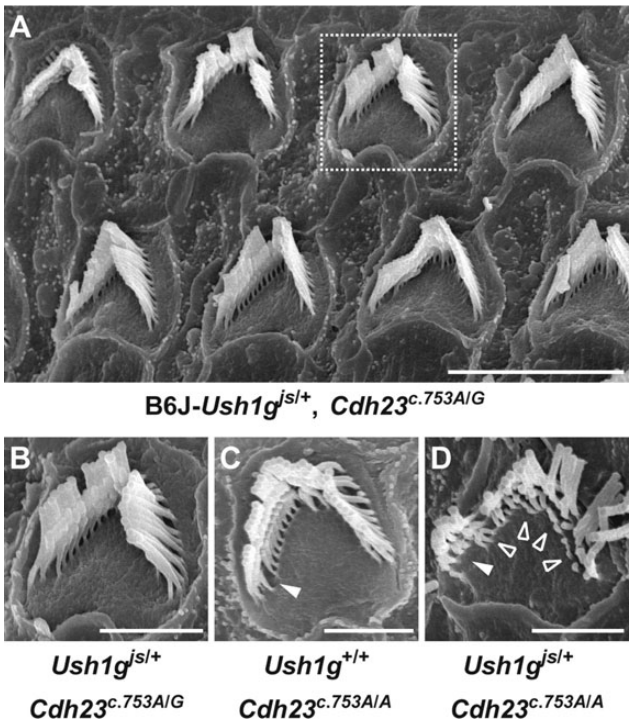

Figure 8. Rescue of the stereocilia degeneration in B6J-*Ush1g*$^{js/+}$ mice by Cas9-mediated *Cdh23*$^{c.753A>G}$ KI. (**A–D**) Representative stereociliary morphology (A) in B6J-*Ush1g*$^{js/+}$, -*Cdh23*$^{c.753A/G}$ double-heterozygous mouse and comparison among the phenotypes of OHC from the middle area in B6J-*Ush1g*$^{js/+}$, -*Cdh23*$^{c.753A/G}$ (B, highly magnified images of the dotted box in A), -*Ush1g*$^{+/+}$, -*Cdh23*$^{c.753A/A}$ (C) and -*Ush1g*$^{js/+}$, -*Cdh23*$^{c.753A/A}$ (D) mice at 6 months of age. The arrowheads and opened arrowheads indicate the absence and shortened of stereocilia, respectively. Scale bars = 5 µm (A) and 2 µm (B–D).

aqueduct syndrome (52). Likewise, hearing loss in patients carrying heterozygous mutations in *USH* genes may require modifier(s) in their genetic background, and strong candidates for such modifiers are mutant alleles present in other *USH* and deafness genes. Therefore, digenic inheritance has been suggested in USH and NSHL patients; double-heterozygous (53–55) and homozygous/heterozygous (56) mutations in two *USH* genes and/or *USH*/modifier genes, respectively, confer the expression and acceleration of hearing loss. Previous mouse studies have reported the digenic inheritance patterns of *Ush* genes (17,55), which is consistent with human cases; our present study also confirmed this and demonstrated the effect of the genetic interaction between the two *Ush* genes on hearing loss at both the nucleotide and sequence levels.

The current study showed that hearing abilities differed among the F_1 mice produced by crossing B6J-*Ush1g*$^{js/js}$ with MSM, D2J, and A/J mice (Figs 2A and 4). The abilities also differed from those of the original strains at different frequencies of sound stimulus. These data strongly suggest the presence of other different dominant modifiers in the genetic backgrounds of mice that affect the hearing phenotype. Similarly to the findings for humans with hearing loss, modifications by single mutant alleles have also been reported in mice (36). Thus, the additive effect of multiple modifiers causing the development and acceleration of hearing loss is a possible scenario in humans.

B6J mice carrying *Cdh23*$^{c.753A}$ alleles are susceptible to AHL, but the C3H and MSM strains are not (40,41). Our study demonstrated that the maintenance of hearing levels over the long term was conferred by the *Cdh23*$^{c.753A>G}$ substitution in B6J mice (Supplementary Material, Fig. S6 and Table S5). This result strongly supports that the homozygosity of *Cdh23*$^{c.753A}$ alleles is primarily responsible for AHL in B6J mice. However, the effect of the hypomorphic *Cdh23*$^{c.753A}$ mutation itself on hearing loss was not as robust because AHL is expressed at a late stage of life in B6J mice (Fig. 1) (15). For the expression of ePHL, additional risk alleles are required, such as *Ush1g*^{js}, *Fscn2*^{ahl8} in D2J mice (47,48) and *Cs*^{ahl4} in A/J mice (49). Similar additional effects of genes related to hearing loss have been reported in mice (40,43,47). When the *Cdh23*$^{c.753A>G}$ substitution was introduced in these mouse models, their hearing ability was restored and maintained over the long term. These data suggest that the homozygosity of the *Cdh23*$^{c.753A}$ allele is a risk factor for ePHL expression.

CDH23 is a component of the tip link, connecting the shorter stereocilia to the shafts of the adjacent, taller stereocilia (6). Previous studies have demonstrated that the wild-type CDH23 protein translated from the unspliced transcript (+ exon 7) localizes to the tip links of stereocilia and that the *Cdh23*$^{c.753A}$ mutation leads to a marked decrease in the expression level of CDH23 in the tip links (15). Hence, it has been suggested that the CDH23 decrease results in the weakening of tip-link tension and the breaking of tip links in mice (15,47,49,57). Moreover, several reports have indicated that the severity of the stereocilia phenotype is increased by the presence of other different mutant alleles, as found in D2J mice (47,48), and by the deletion of the actin, beta gene (*Actb*) in conditional KO (*Actb*$^{flox/flox}$) mice (47). Our results demonstrated the degeneration of stereocilia caused by the additive effect of the combination of a single *Ush1g*^{js} allele with the homozygous *Cdh23*$^{c.753A}$ allele (Fig. 6). More importantly, the observed phenotype was recovered by introducing the *Cdh23*$^{c.753A>G}$ substitution through genome editing (Fig. 8).

The molecular mechanism of the acceleration of the stereocilia defect in *Ush1g*^{js} mice may involve intermolecular interactions between CDH23 and the SANS protein, which is encoded by *Ush1g*. SANS localized to the stereocilia upper tip-link density (UTLD) forms a protein complex, the USH1 interactome, with CDH23 and the other USH1 proteins (5,58). These findings suggest that the stereocilia degeneration observed in B6J-*Ush1g*$^{js/+}$ heterozygous mice may be caused by broken links within the USH1 interactome in the tip link–UTLD as a result of the combined effect of the homozygous *Cdh23*^{ahl} allele and the single *Ush1g*^{js} allele. The interaction between CDH23 and SANS may contribute to stereocilia maintenance at the late stage of life. However, the expression level of CDH23 is extremely low in the tip link and stereocilia of adult mice and rats (15,59,60). Therefore, stereocilia morphogenesis may be incomplete and/or impaired by the disruption of the interaction between CDH23 and SANS, consequently leading to stereocilia degeneration in *Ush1g*$^{js/+}$ mice at an early stage of adulthood.

The degeneration of stereocilia in OHCs was typically more severe than that in IHCs on the hair cells of B6J-*Ush1g*$^{js/+}$ heterozygous mice (Fig. 6L and M). The phenotype of IHC stereocilia in the B6J-*Ush1g*$^{js/js}$ homozygous mice was notably milder than that of OHC stereocilia (Fig. 6A and B) (13,14). Although we cannot explain the molecular mechanisms involved, the interaction between the CDH23 and SANS proteins may have a distinctive role in the development and maintenance of IHCs. Moreover, we found that OHCs in the middle area were more affected than OHCs in the apex area in B6J-*Ush1g*$^{js/+}$ heterozygous mice relative to wild-type B6J-*Ush1g*$^{+/+}$ mice (Fig. 7B and C). This antecedent OHC loss is a typical observation in AHL in mice (38,43,44,50). OHC loss was also detected in both homozygous and heterozygous B6J-*Ush1g* mutants after stereocilia degeneration (Fig. 7A and B). The time course suggests that OHC loss is

likely to be a secondary effect. Oxidative damage (ROS, reactive oxygen species) is a cause of hair cell loss during aging (50,61). Therefore, OHC degeneration in B6J-*Ush1g* mutants may indicate that disrupted stereocilia are more susceptible to ROS, leading to ROS-induced apoptosis of hair cells.

Methods

Mice

B6J-*Ush1g*$^{js/js}$ mice (stock #000783, The Jackson Laboratory, Bar Harbor, ME, USA) and C3H-*Ush1g*$^{seal/seal}$ (13) mice were maintained at the Tokyo Metropolitan Institute of Medical Science by mating homozygous male mice with heterozygous female mice. The control B6J and C3H mice were purchased from CLEA Japan (Tokyo, Japan). To produce genetic crosses, the MSM (62) and B6J-Chr10^{MSM} consomic strain (63) was obtained from the National Institute of Genetics and maintained at the Tokyo Metropolitan Institute of Medical Science. In addition, A/J (Japan SLC, Inc., Hamamatsu, Japan) and D2J (CLEA Japan) female mice were crossed to the B6J and B6J-*Ush1g*$^{js/js}$ mice to perform the genetic analysis of epistasis. All procedures involving animals met the guidelines described in the Proper Conduct of Animal Experiments as defined by the Science Council of Japan and were approved by the Animal Care and Use Committee on the Ethics of the Tokyo Metropolitan Institute of Medical Science (Approval numbers: 13 036, 14 046 and 14 081).

Open-field behavior tests

Mice from each genotype were placed in a 50 cm × 40 cm × 50 cm (W × H × L) open field to quantify behaviors as previously described (15). Data on rotations (times/120 s) and average moving speed (cm/s) were collected for 120 s and analyzed using CompACT VAS software ver. 3.1 (Muromachi Kikai, Tokyo, Japan).

Measurements of ABR

An ABR Workstation (TDT System III, Alachua, FL, USA) was used to test mice for ABR thresholds as previously described (15). The ABR thresholds from both ears in all mice were measured with tone-pip stimuli at 4, 8, 16 and 32 kHz and monthly from 1 to 12 months (±7 days) of age.

Genetic mapping

Genetic mapping of the susceptibility loci in B6J-linked ePHL of *Ush1g*$^{js/+}$ heterozygous mice was performed using intersubspecific N_2 and congenic strains. Progeny of the *Ush1g*$^{js/+}$ heterozygous genotype were selected from [(MSM × B6J-*Ush1g*$^{js/js}$) F_1 × B6J-*Ush1g*$^{js/js}$] N_2 mice by phenotyping, which is the easily identifiable characteristic of normal (*Ush1g*$^{js/+}$) and shaker/waltzer (*Ush1g*$^{js/js}$) behaviors. B6J-*Ush1g*$^{js/+}$, -Chr10^{MSM} congenic mice were produced using the B6J-Chr10^{MSM} consomic strain according to the procedure shown in Supplementary Material, Figure S3. DNA samples from 51 backcross and 105 congenic mice were genotyped using 167 and 19 polymorphic microsatellite markers located throughout the mouse genome and Chr10, respectively (Supplementary Material, Table S6), selected from the Microsatellite Database of Japan (http://www.shigen.nig.ac.jp/mouse/mmdbj/top.jsp, 16 October 2015, date last accessed) based on size variation between PCR products from B6J and MSM mice. The PCR conditions for genotyping were as previously described (44). ABR thresholds at 16 and 32 kHz at 4 months of age (±7 days) were evaluated as quantitative traits for genetic mapping in both backcross and congenic mice. The linkage mappings were performed by QTL interval mapping using the R/qtl program (64) of the R Statistical package and haplotype mapping in the backcross and congenic mice, respectively. The single-QTL genome scans were performed by Haley–Knott regression using a step size of 1.0 cM, and the logarithm of odds (LOD) scores for significance were calculated by 1000 permutations testing using R/qtl.

Generation and characterization of the C57BL/6J-*Ush1g*$^{js/+}$, -*Cdh23*$^{c.753A/G}$ mice

B6J-*Cdh23*$^{c.753A>G}$ KI mice were generated using the CRISPR/Cas9 system. Cas9 plasmid was purchased from Transposagen (Lexington, KY, USA). The Cas9/sgRNA target sequence was designed from the *Cdh23* genomic sequence (Ensembl, GRCm38) and was followed by the underlined PAM sequences: GGACGGGATGTCATGATTGTAG (Supplementary Material, Fig. S4). Template DNA containing the T7 promoter for sgRNA synthesis was prepared by PCR with PF_Cdh23_g60530963-60530983_gR1 and PR_T7 primers (Supplementary Material, Table S3) using the synthetic gene of the guide RNA sequence (65) as a template. PCR amplification was performed using a PrimeSTAR HS DNA Polymerase (Takara Bio, Inc., Kusatsu, Japan) and consisted of 35 cycles at 98°C for 10 s, 56°C for 5 s and 72°C for 15 s. Cas9 mRNA and sgRNA were synthesized using a mMESSAGE mMACHINE T7 ULTRA Transcription Kit (Thermo Fisher Scientific) and MEGAshortscript T7 Transcription Kit (Thermo Fisher Scientific), respectively. Purification and elution of the synthetic RNAs was performed using a MEGAclear Transcription Clean-Up Kit (Thermo Fisher Scientific) and RNase-free water.

Fertilized eggs from B6J were purchased from ARK Resource (Kumamoto, Japan). Cas9 mRNA (10 ng/μl) and transcribed sgRNA (5 ng/μl) and donor oligonucleotide (100 ng/μl, Supplementary Material, Fig. S4 and Supplementary Material, Table S3) were mixed and microinjected into the pronuclei and cytoplasm of fertilized mouse eggs. A total of 309 zygotes were injected with each corresponding Cas9 mRNA/sgRNA/oligonucleotide, and 284 embryos were then transferred to the oviducts of pseudo-pregnant CD1 females (Charles River Laboratories Japan, Yokohama, Japan).

Genomic DNAs were extracted using KAPA Express Extract (Kapa Biosystems, Woburn, MA) from the pinna and tail of the offspring and used for PCR amplification. The target region by the Cas9 nuclease was amplified by using a TaKaRa Ex *Taq* (Takara Bio, Inc.) and a primer pair (Cdh23_g60530682 and Cdh23_g60531255, Supplementary Material, Table S3). After amplification, surveyor assay was performed for all PCR products of the offspring to screen the mutation using the Surveyor Mutation Detection Kit (Transgenomic, Omaha, NE, USA). In addition, PCR products were also analyzed for PCR restriction fragment length polymorphisms (PCR-RFLP) to genotype the *Cdh23*$^{c.753A>G}$ KI. The products were digested with *Msp*I (New England BioLabs, Ipswich, MA, USA) at 37°C for 2–3 h, subjected to 4% agarose (3% Agarose XP and 1% Agarose S, Nippon gene, Tokyo, Japan) gel electrophoresis and stained with ethidium bromide. The *Cdh23*$^{c.753A>G}$ mutation in the screened mice was confirmed by DNA sequencing of the products amplified by a primer pair (Cdh23_g60530706 and Cdh23_g60531304, Supplementary Material, Table S3) using a BigDye Terminator kit (Thermo Fisher Scientific), a Cdh23_g60531255 primer (Supplementary Material, Table S3) and an Applied Biosystems 3500 Genetic Analyzer. Sequence data of *Cdh23* mutants produced by genome editing have been deposited with the GenBank/DDBJ Database under Accession Nos LC094966–094979. Off-target cleavage sites were predicted and searched by CRISPR direct (http://crispr.dbcls.jp/,

11 September 2015, date last accessed). All the potential off-target sites were PCR amplified and sequenced to confirm the off-target effects. The primers for amplifying and sequencing the off-target sites are listed in Supplementary Material, Table S7. The mouse carrying the *Cdh23*$^{c.753G}$ allele was crossed once with B6J mice, and homozygous *Cdh23*$^{c.753G/G}$ KI mice were then produced by sib mating.

Total RNAs were isolated from the inner ears of MSM, B6J, B6J-*Cdh23*$^{c.753A/G}$ heterozygous and B6J-*Cdh23*$^{c.753G/G}$ homozygous mice using the PureLink RNA Mini Kit (Thermo Fisher Scientific) following the manufacturer's protocol. We performed RT-PCR analysis of *Cdh23* as previously described (15) using the *Cdh23* (Cdh23_c433 and Cdh23_c829) and hypoxanthine-guanine phosphoribosyl transferase (*Hprt*) (Hprt_c481 and Hprt_c714) primer sets (Supplementary Material, Table S3).

Scanning electron microscopy

SEM of cochlear stereocilia was performed as described previously (15) in four ears from B6J-*Ush1g*$^{+/+}$ (6 and 10 months of age), -*Ush1g*$^{js/+}$ (1, 3, 6 and 10 months of age), -*Ush1g*$^{js/js}$ (1 month of age), C3H-*Ush1g*$^{+/+}$ (10 months of age), -*Ush1g*$^{seal/+}$ (10 months of age) and B6J-*Ush1g*$^{js/+}$, *Cdh23*$^{c.753A/G}$ (6 months of age) mice and examined using a Hitachi S-4800 field emission scanning electron microscope at an accelerating voltage of 10 kV.

Hair cell counts

Cochlea from B6J-*Ush1g*$^{+/+}$ (6 months of age, $n = 4$; 9 months of age, $n = 4$; 12 months of age, $n = 3$), -*Ush1g*$^{js/+}$ (6 months of age, $n = 4$; 9 months of age, $n = 3$; 12 months of age, $n = 4$), -*Ush1g*$^{js/js}$ (1 months of age, $n = 4$; 3 months of age, $n = 3$; 6 months of age, EZW094TB2$n = 4$), C3H-*Ush1g*$^{seal/+}$ ($n = 2$; 12 months of age) and B6J-*Ush1g*$^{js/+}$, *Cdh23*$^{c.753A/G}$ ($n = 4$; 6 months of age) mice were used for whole-mount immunohistochemistry using an anti-MYO6 antibody (0.5 μg/ml, Proteus BioSciences, Ramona, CA, USA) and Alexa Fluor 488 phalloidin (0.2 μM, Thermo Fisher Scientific, Waltham, MA, USA). Whole-mount immunohistochemistry was performed as previously described (15). Hair cell images were obtained with a Zeiss LSM510 confocal microscope (Carl Zeiss, Jena, Germany). The signals of both MYO6 and phalloidin were counted in the regions of 100 μm within areas 1 (1.2–1.5 mm) and 2 (2.1–2.4 mm) from the apex in the oC of each mouse (Supplementary Material, Fig. S9).

Statistical analyses

All results are presented as the mean ± standard deviation (SD). Differences among multiple groups were analyzed by one-way ANOVA with Tukey's *post hoc* multiple comparison test. The two groups were compared using Student's *t*-test with Welch's correction. GraphPad Prism 5 (GraphPad, San Diego, CA, USA) was used to calculate column statistics and compute *P*-values.

Supplementary Material

Supplementary Material is available at *HMG* online.

Acknowledgements

We thank Takuya Ueda, Yoshihiko Sagara, Yusuke Sakuma and Yo Obara for technical assistance.

Conflict of Interest statement. None declared.

Funding

This work was supported by Japan Society for the Promotion of Science KAKENHI (Grants-in-Aid for Scientific Research B) (Grant Numbers 20300147, 23300160 and 15H04291 to Y.K.) and (Grants-in-Aid for JSPS Fellows) (Grant Number 14J06119 to Y.M.).

References

1. Keats, B.J.B. and Lentz, J. (1999, updated 2013) Usher syndrome type I. In Pagon, R.A., Adam, M.P., Ardinger, H.H., Wallace, S.E., Amemiya, A., Bean, L.J.H., Bird, T.D., Fong, C.T., Mefford, H.C., Smith, R.J.H. and Stephens, K. (eds), Gene Reviews *(Internet)*, University of Washington, Seattle, WA.
2. Yan, D. and Liu, X.Z. (2010) Genetics and pathological mechanisms of Usher syndrome. *J. Hum. Genet.*, **55**, 327–335.
3. Puffenberger, E.G., Jinks, R.N., Sougnez, C., Cibulskis, K., Willert, R.A., Achilly, N.P., Cassidy, R.P., Fiorentini, C.J., Heiken, K.F., Lawrence, J.J. *et al.* (2012) Genetic mapping and exome sequencing identify variants associated with five novel diseases. *PLoS One*, **7**, e28936.
4. Geng, R., Melki, S., Chen, D.H., Tian, G., Furness, D.N., Oshima-Takago, T., Neef, J., Moser, T., Askew, C., Horwitz, G. *et al.* (2012) The mechanosensory structure of the hair cell requires clarin-1, a protein encoded by Usher syndrome III causative gene. *J. Neurosci.*, **32**, 9485–9498.
5. Grati, M. and Kachar, B. (2011) Myosin VIIa and sans localization at stereocilia upper tip-link density implicates these Usher syndrome proteins in mechanotransduction. *Proc. Natl. Acad. Sci. USA*, **108**, 11476–11481.
6. Kazmierczak, P., Sakaguchi, H., Tokita, J., Wilson-Kubalek, E.M., Milligan, R.A., Müller, U. and Kachar, B. (2007) Cadherin 23 and protocadherin 15 interact to form tip-link filaments in sensory hair cells. *Nature*, **449**, 87–91.
7. Lefèvre, G., Michel, V., Weil, D., Lepelletier, L., Bizard, E., Wolfrum, U., Hardelin, J.P. and Petit, C. (2008) A core cochlear phenotype in USH1 mouse mutants implicates fibrous links of the hair bundle in its cohesion, orientation and differential growth. *Development*, **135**, 1427–1437.
8. Liu, X., Bulgakov, O.V., Darrow, K.N., Pawlyk, B., Adamian, M., Liberman, M.C. and Li, T. (2007) Usherin is required for maintenance of retinal photoreceptors and normal development of cochlear hair cells. *Proc. Natl. Acad. Sci. USA*, **104**, 4413–4418.
9. Mathur, P.D., Zou, J., Zheng, T., Almishaal, A., Wangm, Y., Chen, Q., Wang, L., Vashist, D., Brown, S., Park, A. *et al.* (2015) Distinct expression and function of whirlin isoforms in the inner ear and retina: an insight into pathogenesis of USH2D and DFNB31. *Hum. Mol. Genet.*, **24**, 6213–6228.
10. McGee, J., Goodyear, R.J., McMillan, D.R., Stauffer, E.A., Holt, J.R., Locke, K.G., Birch, D.G., Legan, P.K., White, P.C., Walsh, E.J. *et al.* (2006) The very large G-protein-coupled receptor VLGR1: a component of the ankle link complex required for the normal development of auditory hair bundles. *J. Neurosci.*, **26**, 6543–6553.
11. Riazuddin, S., Belyantseva, I.A., Giese, A.P., Lee, K., Indzhykulian, A.A., Nandamuri, S.P., Yousaf, R., Sinha, G.P., Lee, S., Terrell, D. *et al.* (2012) Alterations of the CIB2 calcium- and integrin-binding protein cause Usher syndrome type 1J and nonsyndromic deafness DFNB48. *Nat. Genet.*, **44**, 1265–1271.
12. Di Palma, F., Holme, R.H., Bryda, E.C., Belyantseva, I.A., Pellegrino, R., Kachar, B., Steel, K.P. and Noben-Trauth, K. (2001) Mutations in *Cdh23*, encoding a new type of cadherin, cause stereocilia disorganization in waltzer, the mouse model for Usher syndrome type 1D. *Nat. Genet.*, **27**, 103–107.

13. Kikkawa, Y., Shitara, H., Wakana, S., Kohara, Y., Takada, T., Okamoto, M., Taya, C., Kamiya, K., Yoshikawa, Y., Tokano, H. *et al.* (2003) Mutations in a new scaffold protein *Sans* cause deafness in Jackson shaker mice. *Hum. Mol. Genet.*, **12**, 453–461.
14. Kitamura, K., Kakoi, H., Yoshikawa, Y. and Ochikubo, F. (1992) Ultrastructural findings in the inner ear of Jackson shaker mice. *Acta. Otolaryngol.*, **112**, 622–627.
15. Miyasaka, Y., Suzuki, S., Ohshiba, Y., Watanabe, K., Sagara, Y., Yasuda, S.P., Matsuoka, K., Shitara, H., Yonekawa, H., Kominami, R. *et al.* (2013) Compound heterozygosity of the functionally null *Cdh23*$^{v\text{-}ngt}$ and hypomorphic *Cdh23*^{ahl} alleles leads to early-onset progressive hearing loss in mice. *Exp. Anim.*, **62**, 333–346.
16. Self, T., Mahony, M., Fleming, J., Walsh, J., Brown, S.D. and Steel, K.P. (1998) Shaker-1 mutations reveal roles for myosin VIIA in both development and function of cochlear hair cells. *Development*, **125**, 557–566.
17. Zheng, Q.Y., Scarborough, J.D., Zheng, Y., Yu, H., Choi, D. and Gillespie, P.G. (2012) Digenic inheritance of deafness caused by 8J allele of myosin-VIIA and mutations in other Usher I genes. *Hum. Mol. Genet.*, **21**, 2588–2598.
18. Liu, X.Z., Walsh, J., Mburu, P., Kendrick-Jones, J., Cope, M.J., Steel, K.P. and Brown, S.D. (1997) Mutations in the myosin VIIA gene cause non-syndromic recessive deafness. *Nat. Genet.*, **16**, 188–190.
19. Ahmed, Z.M., Smith, T.N., Riazuddin, S., Makishima, T., Ghosh, M., Bokhari, S., Menon, P.S., Deshmukh, D., Griffith, A.J., Riazuddin, S. *et al.* (2002) Nonsyndromic recessive deafness DFNB18 and Usher syndrome type IC are allelic mutations of USHIC. *Hum. Genet.*, **110**, 527–531.
20. Bork, J.M., Peters, L.M., Riazuddin, S., Bernstein, S.L., Ahmed, Z.M., Ness, S.L., Polomeno, R., Ramesh, A., Schloss, M., Srisailpathy, C.R. *et al.* (2001) Usher syndrome 1D and nonsyndromic autosomal recessive deafness DFNB12 are caused by allelic mutations of the novel cadherin-like gene *CDH23*. *Am. J. Hum. Genet.*, **68**, 26–37.
21. Ahmed, Z.M., Riazuddin, S., Ahmad, J., Bernstein, S.L., Guo, Y., Sabar, M.F., Sieving, P., Riazuddin, S., Griffith, A.J., Friedman, T.B. *et al.* (2003) *PCDH15* is expressed in the neurosensory epithelium of the eye and ear and mutant alleles are responsible for both USH1F and DFNB23. *Hum. Mol. Genet.*, **12**, 3215–3223.
22. Maria Oonk, A.M., van Huet, R.A., Leijendeckers, J.M., Oostrik, J., Venselaar, H., van Wijk, E., Beynon, A., Kunst, H.P., Hoyng, C.B., Kremer, H. *et al.* (2015) Nonsyndromic hearing loss caused by *USH1G* mutations: widening the *USH1G* disease spectrum. *Ear Hear.*, **36**, 205–211.
23. Mburu, P., Mustapha, M., Varela, A., Weil, D., El-Amraoui, A., Holme, R.H., Rump, A., Hardisty, R.E., Blanchard, S., Coimbra, R.S. *et al.* (2003) Defects in whirlin, a PDZ domain molecule involved in stereocilia elongation, cause deafness in the whirler mouse and families with DFNB31. *Nat. Genet.*, **34**, 421–428.
24. Liu, X.Z., Walsh, J., Tamagawa, Y., Kitamura, K., Nishizawa, M., Steel, K.P. and Brown, S.D.M. (1997) Autosomal dominant non-syndromic deafness caused by a mutation in the myosin VIIA gene. *Nat. Genet.*, **17**, 268–269.
25. Luijendijk, M.W.J., van Wijk, E., Bischoff, A.M.L.C., Krieger, E., Huygen, P.L.M., Pennings, R.J.E., Brunner, H.G., Cremers, C.W. R.J., Cremers, F.P.M. and Kremer, H. (2004) Identification and molecular modelling of a mutation in the motor head domain of myosin VIIA in a family with autosomal dominant hearing impairment (DFNA11). *Hum. Genet.*, **115**, 149–156.
26. Sun, Y., Chen, J., Sun, H., Cheng, J., Li, J., Lu, Y., Lu, Y., Jin, Z., Zhu, Y., Ouyang, X. *et al.* (2011) Novel missense mutations in MYO7A underlying postlingual high- or low-frequency non-syndromic hearing impairment in two large families from China. *J. Hum. Genet.*, **56**, 64–70.
27. Ganapathy, A., Pandey, N., Srisailapathy, C.R., Jalvi, R., Malhotra, V., Venkatappa, M., Chatterjee, A., Sharma, M., Santhanam, R., Chadha, S. *et al.* (2014) Non-syndromic hearing impairment in India: high allelic heterogeneity among mutations in *TMPRSS3*, *TMC1*, *USHIC*, *CDH23* and *TMIE*. *PLoS One*, **9**, e84773.
28. Miyagawa, M., Nishio, S.Y. and Usami, S. (2012) Prevalence and clinical features of hearing loss patients with *CDH23* mutations: a large cohort study. *PLoS One*, **7**, e40366.
29. Chen, D.Y., Zhu, W.D., Chai, Y.C., Chen, Y., Sun, L., Yang, T. and Wu, H. (2015) Mutation in *PCDH15* may modify the phenotypic expression of the 7511T>C mutation in *MT-TS1* in a Chinese Han family with maternally inherited nonsyndromic hearing loss. *Int. J. Pediatr. Otorhinolaryngol.*, **79**, 1654–1657.
30. Kubisch, C., Schroeder, B.C., Friedrich, T., Lutjohann, B., El-Amraoui, A., Marlin, S., Petit, C. and Jentsch, T.J. (1999) *KCNQ4*, a novel potassium channel expressed in sensory outer hair cells, is mutated in dominant deafness. *Cell*, **96**, 437–446.
31. Mencia, A., Gonzalez-Nieto, D., Modamio-Hoybjor, S., Etxeberria, A., Aranguez, G., Salvador, N., del Castillo, I., Villarroel, A., Moreno, F., Barrio, L. *et al.* (2008) Novel *KCNQ4* pore-region mutation (p.G296S) causes deafness by impairing cell-surface channel expression. *Hum. Genet.*, **123**, 41–53.
32. Morin, M., Bryan, K.E., Mayo-Merino, F., Goodyear, R., Mencia, A., Modamio-Hoybjor, S., del Castillo, I., Cabalka, J.M., Richardson, G., Moreno, F. *et al.* (2009) *In vivo* and *in vitro* effects of two novel gamma-actin (*ACTG1*) mutations that cause DFNA20/26 hearing impairment. *Hum. Mol. Genet.*, **18**, 3075–3089.
33. Zhu, M., Yang, T., Wei, S., DeWan, A.T., Morell, R.J., Elfenbein, J.L., Fisher, R.A., Leal, S.M., Smith, R.J.H. and Friderici, K.H. (2003) Mutations in the gamma-actin gene (*ACTG1*) are associated with dominant progressive deafness (DFNA20/26). *Am. J. Hum. Genet.*, **73**, 1082–1091.
34. Kochhar, A., Hildebrand, M.S. and Smith, R.J. (2007) Clinical aspects of hereditary hearing loss. *Genet. Med.*, **9**, 393–408.
35. Smith, R.J.H., Shearer, A.E., Hildebrand, M.S. and Van Camp, G. (1993, updated 2014) Deafness and hereditary hearing loss overview. In Pagon, R.A., Adam, M.P., Ardinger, H.H., Wallace, S.E., Amemiya, A., Bean, L.J.H., Bird, T.D., Fong, C.T., Mefford, H.C., Smith, R.J.H. *et al.* (eds), GeneReviews *(Internet)*, University of Washington, Seattle, WA.
36. Yan, D. and Liu, X.Z. (2010) Modifiers of hearing impairment in humans and mice. *Curr. Genomics*, **11**, 269–278.
37. Vona, B., Müller, T., Nanda, I., Neuner, C., Hofrichter, M.A., Schröder, J., Bartsch, O., Läßig, A., Keilmann, A., Schraven, S. *et al.* (2014) Targeted next-generation sequencing of deafness genes in hearing-impaired individuals uncovers informative mutations. *Genet. Med.*, **16**, 945–953.
38. Ohlemiller, K.K. (2006) Contributions of mouse models to understanding of age- and noise-related hearing loss. *Brain Res.*, **1091**, 89–102.
39. Kaneko, T. and Mashimo, T. (2015) Creating knockout and knockin rodents using engineered endonucleases via direct embryo injection. *Methods Mol. Biol.*, **1239**, 307–315.
40. Noben-Trauth, K., Zheng, Q.Y. and Johnson, K.R. (2003) Association of cadherin 23 with polygenic inheritance and genetic modification of sensorineural hearing loss. *Nat. Genet.*, **35**, 21–23.

41. Nemoto, M., Morita, Y., Mishima, Y., Takahashi, S., Nomura, T., Ushiki, T., Shiroishi, T., Kikkawa, Y., Yonekawa, H. and Kominami, R. (2004) *Ahl3*, a third locus on mouse chromosome 17 affecting age-related hearing loss. *Biochem. Biophys. Res. Commun.*, **324**, 1283–1288.
42. Johnson, K.R., Longo-Guess, C., Gagnon, L.H., Yu, H. and Zheng, Q.Y. (2008) A locus on distal chromosome 11 (*ahl8*) and its interaction with $Cdh23^{ahl}$ underlie the early onset, age-related hearing loss of DBA/2J mice. *Genomics*, **92**, 219–225.
43. Johnson, K.R., Yu, H., Ding, D., Jiang, H., Gagnon, L.H. and Salvi, R.J. (2010) Separate and combined effects of *Sod1* and *Cdh23* mutations on age-related hearing loss and cochlear pathology in C57BL/6J mice. *Hear. Res.*, **268**, 85–92.
44. Suzuki, S., Ishikawa, M., Ueda, T., Ohshiba, Y., Miyasaka, Y., Okumura, K., Yokohama, M., Taya, C., Matsuoka, K. and Kikkawa, Y. (2015) Quantitative trait loci on chromosome 5 for susceptibility to frequency-specific effects on hearing in DBA/2J mice. *Exp. Anim.*, **64**, 241–251.
45. Zheng, Q.Y., Ding, D., Yu, H., Salvi, R.J. and Johnson, K.R. (2009) A locus on distal chromosome 10 (*ahl4*) affecting age-related hearing loss in A/J mice. *Neurobiol. Aging*, **30**, 1693–1705.
46. Haines, J.L. and Pericak-Vance, M.A. (2006) Genetic Analysis of Complex Diseases *(2nd Edition)*, Wiley & Sons, Hoboken, NJ.
47. Perrin, B.J., Strandjord, D.M., Narayanan, P., Henderson, D.M., Johnson, K.R. and Ervasti, J.M. (2013) β-Actin and fascin-2 cooperate to maintain stereocilia length. *J. Neurosci.*, **33**, 8114–8121.
48. Shin, J.B., Longo-Guess, C.M., Gagnon, L.H., Saylor, K.W., Dumont, R.A., Spinelli, K.J., Pagana, J.M., Wilmarth, P.A., David, L.L., Gillespie, P.G. *et al.* (2010) The R109H variant of fascin-2, a developmentally regulated actin crosslinker in hair-cell stereocilia, underlies early-onset hearing loss of DBA/2J mice. *J. Neurosci.*, **30**, 9683–9694.
49. Johnson, K.R., Gagnon, L.H., Longo-Guess, C. and Kane, K.L. (2012) Association of a citrate synthase missense mutation with age-related hearing loss in A/J mice. *Neurobiol. Aging*, **33**, 1720–1729.
50. Someya, S., Xu, J., Kondo, K., Ding, D., Salvi, R.J., Yamasoba, T., Rabinovitch, P.S., Weindruch, R., Leeuwenburgh, C., Tanokura, M. *et al.* (2009) Age-related hearing loss in C57BL/6J mice is mediated by Bak-dependent mitochondrial apoptosis. *Proc. Natl. Acad. Sci. USA*, **106**, 19432–19437.
51. Liu, X.Z., Yuan, Y., Yan, D., Ding, E.H., Ouyang, X.M., Fei, Y., Tang, W., Yuan, H., Chang, Q., Du, L.L. *et al.* (2009) Digenic inheritance of non-syndromic deafness caused by mutations at the gap junction proteins Cx26 and Cx31. *Hum. Genet.*, **125**, 53–62.
52. Yang, T., Gurrola, J.G. II, Wu, H., Chiu, S.M., Wangemann, P., Snyder, P.M. and Smith, R.J. (2009) Mutations of *KCNJ10* together with mutations of *SLC26A4* cause digenic nonsyndromic hearing loss associated with enlarged vestibular aqueduct syndrome. *Am. J. Hum. Genet.*, **84**, 651–657.
53. Aparisi, M.J., Aller, E., Fuster-García, C., García-García, G., Rodrigo, R., Vázquez-Manrique, R.P., Blanco-Kelly, F., Ayuso, C., Roux, A.F., Jaijo, T. *et al.* (2014) Targeted next generation sequencing for molecular diagnosis of Usher syndrome. *Orphanet. J. Rare Dis.*, **9**, 168.
54. Yoshimura, H., Iwasaki, S., Nishio, S.Y., Kumakawa, K., Tono, T., Kobayashi, Y., Sato, H., Nagai, K., Ishikawa, K., Ikezono, T. *et al.* (2014) Massively parallel DNA sequencing facilitates diagnosis of patients with Usher syndrome type 1. *PLoS One*, **9**, e90688.
55. Zheng, Q.Y., Yan, D., Ouyang, X.M., Du, L.L., Yu, H., Chang, B., Johnson, K.R. and Liu, X.Z. (2005) Digenic inheritance of deafness caused by mutations in genes encoding cadherin 23 and protocadherin 15 in mice and humans. *Hum. Mol. Genet.*, **14**, 103–111.
56. Ebermann, I., Phillips, J.B., Liebau, M.C., Koenekoop, R.K., Schermer, B., Lopez, I., Schäfer, E., Roux, A.F., Dafinger, C., Bernd, A. *et al.* (2010) *PDZD7* is a modifier of retinal disease and a contributor to digenic Usher syndrome. *J. Clin. Invest.*, **120**, 1812–1823.
57. Schwander, M., Xiong, W., Tokita, J., Lelli, A., Elledge, H.M., Kazmierczak, P., Sczaniecka, A., Kolatkar, A., Wiltshire, T., Kuhn, P. *et al.* (2009) A mouse model for nonsyndromic deafness (DFNB12) links hearing loss to defects in tip links of mechanosensory hair cells. *Proc. Natl. Acad. Sci. USA*, **106**, 5252–5257.
58. Adato, A., Michel, V., Kikkawa, Y., Reiners, J., Alagramam, K.N., Weil, D., Yonekawa, H., Wolfrum, U., El-Amraoui, A. and Petit, C. (2005) Interactions in the network of Usher syndrome type 1 proteins. *Hum. Mol. Genet.*, **14**, 347–356.
59. Lagziel, A., Ahmed, Z.M., Schultz, J.M., Morell, R.J., Belyantseva, I.A. and Friedman, T.B. (2005) Spatiotemporal pattern and isoforms of cadherin 23 in wild type and waltzer mice during inner ear hair cell development. *Dev. Biol.*, **280**, 295–306.
60. Michel, V., Goodyear, R.J., Weil, D., Marcotti, W., Perfettini, I., Wolfrum, U., Kros, C.J., Richardson, G.P. and Petit, C. (2005) Cadherin 23 is a component of the transient lateral links in the developing hair bundles of cochlear sensory cells. *Dev. Biol.*, **280**, 281–294.
61. Someya, S., Yu, W., Hallows, W.C., Xu, J., Vann, J.M., Leeuwenburgh, C., Tanokura, M., Denu, J.M. and Prolla, T.A. (2010) *Sirt3* mediates reduction of oxidative damage and prevention of age-related hearing loss under caloric restriction. *Cell*, **143**, 802–812.
62. Moriwaki, K., Miyashita, N., Mita, A., Gotoh, H., Tsuchiya, K., Kato, H., Mekada, K., Noro, C., Oota, S., Yoshiki, A. *et al.* (2009) Unique inbred strain MSM/Ms established from the Japanese wild mouse. *Exp. Anim.*, **58**, 123–134.
63. Takada, T., Mita, A., Maeno, A., Sakai, T., Shitara, H., Kikkawa, Y., Moriwaki, K., Yonekawa, H. and Shiroishi, T. (2008) Mouse inter-subspecific consomic strains for genetic dissection of quantitative complex traits. *Genome Res.*, **18**, 500–508.
64. Broman, K.W. and Sen, Ś. (2009) *A Guide to QTL Mapping with R/qtl*. Springer, New York, NY.
65. Hwang, W.Y., Fu, Y., Reyon, D., Maeder, M.L., Tsai, S.Q., Sander, J.D., Peterson, R.T., Yeh, J.R. and Joung, J.K. (2013) Efficient genome editing in zebrafish using a CRISPR-Cas system. *Nat. Biotechnol.*, **3**, 227–229.